THE SOLAR OSCILLATIONS INVESTIGATION – MICHELSON DOPPLER IMAGER

P.H. SCHERRER, R.S. BOGART, R.I. BUSH, J.T. HOEKSEMA, A.G. KOSOVICHEV and J. SCHOU
W.W. Hansen Experimental Physics Laboratory, Center for Space Science and Astrophysics, Stanford University, Stanford, CA 94305-4085.

and

W. ROSENBERG, L. SPRINGER, T.D. TARBELL, A. TITLE, C.J. WOLFSON, I. ZAYER and THE MDI ENGINEERING TEAM*
Lockheed Palo Alto Research Laboratory 91-30/252, 3251 Hanover St., Palo Alto, CA 94304.

Abstract. The Solar Oscillations Investigation (SOI) uses the Michelson Doppler Imager (MDI) instrument to probe the interior of the Sun by measuring the photospheric manifestations of solar oscillations. Characteristics of the modes reveal the static and dynamic properties of the convection zone and core. Knowledge of these properties will improve our understanding of the solar cycle and of stellar evolution. Other photospheric observations will contribute to our knowledge of the solar magnetic field and surface motions. The investigation consists of coordinated efforts by several teams pursuing specific scientific objectives.

The instrument images the Sun on a 1024^2 CCD camera through a series of increasingly narrow spectral filters. The final elements, a pair of tunable Michelson interferometers, enable MDI to record filtergrams with a FWHM bandwidth of 94 mÅ. Normally 20 images centered at 5 wavelengths near the Ni I 6768 spectral line are recorded each minute. MDI calculates velocity and continuum intensity from the filtergrams with a resolution of $4''$ over the whole disk. An extensive calibration program has verified the end-to-end performance of the instrument.

To provide continuous observations of the longest-lived modes that reveal the internal structure of the Sun, a carefully-selected set of spatial averages are computed and downlinked at all times. About half the time MDI will also be able to downlink complete velocity and intensity images each minute. This high rate telemetry (HRT) coverage is available for at least a continuous 60-day interval each year and for 8 hours each day during the rest of the year. During the 8-hour HRT intervals, 10 of the exposures each minute can be programmed for other observations, such as measurements in MDI's higher resolution ($1.25''$) field centered about $160''$ north of the equator; meanwhile, the continuous structure program proceeds during the other half minute. Several times each day, polarizers will be inserted to measure the line-of-sight magnetic field.

MDI operations will be scheduled well in advance and will vary only during the daily 8-hour campaigns. Quick-look and summary data, including magnetograms, will be processed immediately. Most high-rate data will be delivered only by mail to the SOI Science Support Center (SSSC) at Stanford, where a processing pipeline will produce 3 Terabytes of calibrated data products each year. These data products will be analyzed using the SSSC and the distributed resources of the co-investigators. The data will be available for collaborative investigations.

* The MDI Engineering Team leaders include: D. Akin, B. Carvalho, R. Chevalier, D. Duncan, C. Edwards, N. Katz, M. Levay, R. Lindgren, D. Mathur, S. Morrison, T. Pope, R. Rehse, and D. Torgerson.

Solar Physics **162**: 129–188, 1995.

1. Introduction

The SOHO mission (Domingo *et al.*, 1995) emphasizes three principal areas of scientific investigation: (1) probing the solar interior using the techniques of helioseismology, (2) determining the heating mechanism of the solar corona, and (3) studying the solar wind and its acceleration process. Instruments of three SOHO teams perform helioseismology measurements: GOLF (Global Oscillations at Low Frequencies, Gabriel *et al.*, 1995), VIRGO (Variability of IRradiance and Gravity Oscillations, Fröhlich *et al.*, 1995) and SOI (the Solar Oscillations Investigation). This paper describes the SOI program and the Michelson Doppler Imager (MDI) instrument it uses. The requirements of the helioseismology experiments are in part responsible for some of the key characteristics of the SOHO spacecraft. The high rate telemetry capability satisfies the MDI requirements, the need for a small range in SOHO-Sun radial velocity meets the needs of GOLF and MDI, and continuous sunlight supports all three experiments.

In 1960 Leighton, Noyes & Simon (1962) discovered the solar 5-minute oscillations of the vertical motion of the photosphere. A decade later Ulrich (1970) and Leibacher & Stein (1971) independently proposed the hypothesis that these oscillations were the result of acoustic-gravity waves trapped below the photosphere. The first observations demonstrating that the relationship between the horizontal wavelength and frequency of the oscillations agreed well with theory were made by Deubner (1975). It was soon realized that these trapped waves could be used to probe the interior structure of the Sun and the field of helioseismology was born, although that term, suggested by D. Gough, was not generally adopted until 1983. The early observations were an astonishing accomplishment, but the data suffered from the fundamental limitations of all ground-based helioseismological efforts: distortions caused by atmospheric turbulence and gaps caused by the day-night cycle and poor weather.

Two approaches have been and are being followed on the ground to deal with the data gap problem. Observations from the South Pole during the Antarctic summer provide multiple-day runs of continuous viewing (e.g., Duvall *et al.*, 1991, Grec *et al.*, 1980). Analysis of these data have been crucial to advancing our knowledge of the solar interior. Longer uninterrupted data series can be obtained by combining data from a network of sites at different longitudes. This is being done by a number of groups, GONG (Harvey *et al.*, 1988) being most similar to SOI. However, atmospheric turbulence imposes fundamental limitations on ground-based observations. Detailed investigations of high-degree modes need better spatial resolution and small-amplitude low-frequency modes need higher signal-to-noise, requiring spaceborne instrumentation (Noyes & Rhodes, 1984).

Formal study of the potential for doing helioseismology from space began in 1978 when J.D. Bohlin of NASA commissioned a Science Working Group (SWG), chaired by G.A. Newkirk, Jr., to determine the best space mission(s) to follow the Solar Maximum Mission. The concept was endorsed by the Astronomy Survey Committee (Field *et al.*, 1982) and by the Committee on Solar and Space Physics (Krimigis *et al.*, 1985). Meanwhile, NASA established a second SWG to specifically consider helioseismology from space, with R. Canfield as the initial chairman and then R.W. Noyes as the permanent chairman. The report of this SWG (Noyes and Rhodes, 1984) recommended that NASA develop "a space-qualified two-dimensional solar imager capable of measuring velocities" and fly it "in a fully or nearly fully sunlit orbit, such as a halo orbit around the Lagrangian L_1 point." The SWG also endorsed "complementary acquisition and analysis of helioseismology data from ground-based observatories or networks of observing stations." Meanwhile, in Europe there were several studies leading to proposals for space missions to study the low-degree oscillations that probe the deep interior, e.g., DISCO. The SOHO mission encompasses the U.S. and European helioseismology goals as well as other common solar aims.

A joint ESA/NASA Announcement of Opportunity to participate in the SOHO mission was issued in March 1987. The proposal of the SOI-MDI team, led by P. H. Scherrer of Stanford University, was selected for further definition later that year, and in January 1988, a revised proposal, including some instrument descopes, was submitted. On 11 March 1988, SOI-MDI was selected for development and in October 1990, after a low-level definition phase was completed, full-scale development commenced. The next few years saw refinements in the instrument design and maturation of the scientific program. Various difficulties were encountered and overcome, and the flight instrument was delivered for interface testing in January 1994. After a brief return to Palo Alto to incorporate some improvements and perform additional calibrations, final delivery of MDI took place on 28 April 1994.

Many scientists from throughout the world have contributed to the creation and development of SOI-MDI, are participating in the science preparations, and will cooperate in the operations and data collection, reduction, and analysis. Most of the MDI instrument development took place under the direction of A.M. Title at the Lockheed Palo Alto Research Laboratory. The development of the SOI data analysis facility and the overall coordination of the science investigation has been directed by P. H. Scherrer at Stanford.

Investigators participating in the SOI-MDI project, as of May 1995, include: P.H. Scherrer (PI), T. Bai, T. Berger, R.S. Bogart, R.N. Bracewell, R.I. Bush, T.L. Duvall, Jr., J.T. Hoeksema, A.G. Kosovichev, P. Milford, J. Schou, P. Sturrock, A.B.C. Walker, Jr. (CoI), and X.P. Zhao at Stanford University; A.M. Title (CoI), N. Hurlburt, C.J. Schrijver, R.A. Shine, T.D. Tarbell (CoI), C.J. Wolfson, and I. Zayer at Lockheed Palo Alto Research

Labs; J. Christensen-Dalsgaard (CoI) at Aarhus Universitet; K.G. Libbrecht (CoI) at the California Institute of Technology; D.O. Gough (CoI), and T. Sekii at the University of Cambridge; J.W. Leibacher (CoI), K. Bachmann, J.W. Harvey, F. Hill, and J.R. Kennedy at the National Solar Observatory; J.R. Kuhn (CoI) at Michigan State University and NSO; T.M. Brown (CoI) at NCAR's High Altitude Observatory; R.W. Noyes (CoI) and S. Korzennik at the Smithsonian Astrophysical Observatory; R.K. Ulrich (CoI) at the University of California at Los Angeles; J. Toomre (CoI), E.G. Zweibel (CoI), D.A. Haber, K. Julien, and R. Stebbins at the University of Colorado; and E.J. Rhodes, Jr. (CoI) and W. Däppen at the University of Southern California. Scientists at other institutions include B. Andersen, T. Appourchaux, M. Brodsky, J.C. Brown, A. Cacciani, P. Delache (deceased), E. Fossat, C. Fröhlich, B. Gelly, D. Hathaway, S. Horner, V. Kotov, J. Lawrence, W. Merryfield, J. Pap, G. Price, D.M. Rust, R. Rutten, A. Ruzmaikin, H. Shibahashi, G.W. Simon, H. Snodgrass, J. Stenflo, M.J. Thompson, M. Woodard, and H. Yoshimura.

The remainder of this paper summarizes the SOI scientific objectives, explains the operation of the science teams, describes the MDI instrument developed to make the required measurements, and presents the instrument's measured and anticipated performance. It also describes the specific scientific observing programs, the plans for mission operations, and the facilities and capabilities for data reduction and analysis that will link the data collection and scientific analysis efforts. This information is directed to everyone who will participate in the SOI-MDI program, and we hope it will encourage the participation of many new individuals. It is not, however, a Users' Manual nor does it provide details of instrumental "quirks" and calibrations.

2. The SOI Science Program

The primary goal of SOI is to understand the interior structure and dynamics of the Sun using the techniques of helioseismology. Before discussing the particular science goals of SOI, we briefly introduce the MDI observing strategy and examine the domains in the solar interior that are accessible via helioseismology (for a recent review, see Gough & Toomre, 1991).

2.1. MDI Observing Strategy

MDI is sensitive to the three principal classes of oscillations: acoustic waves (p modes), internal gravity waves (g modes), and surface gravity waves (f modes). Each mode is trapped in a particular region of the Sun and the nature of the oscillation depends principally on the structure of the Sun in that region. The most useful measurement is the mode frequency, but measurements of the relative phases of velocity and intensity and of mode amplitudes also provide important diagnostic information. MDI determines

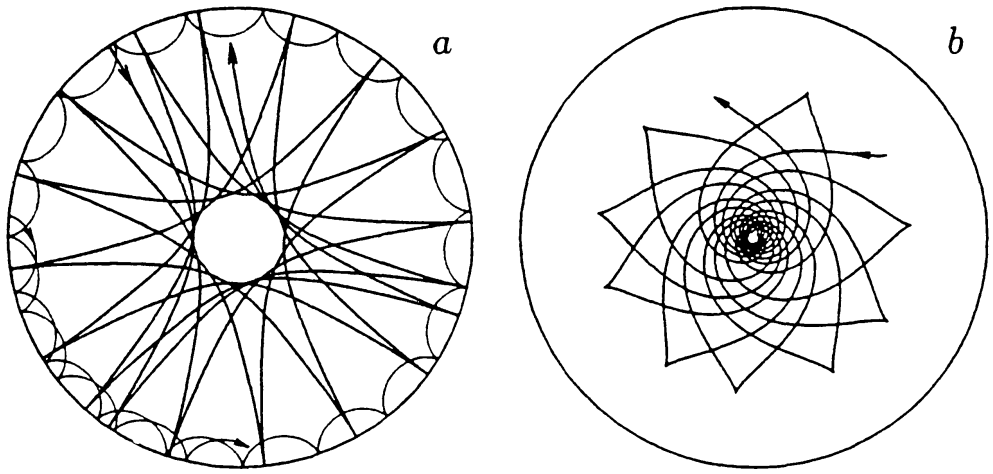

Fig. 1. Ray paths for representative acoustic and gravity waves in a standard model Sun (from Gough & Toomre, 1991). The acoustic modes (panel a) probe different parts of the Sun; $p_8(\ell = 100)$ penetrates less deeply than $p_8(\ell = 2)$. The $g_{10}(\ell = 5)$ mode (panel b) is confined mainly to the deep interior. (Reproduced, with permission, from the *Annual Review Astronomy and Astrophysics* , Volume 29, ©1991, by Annual Reviews Inc.)

mode properties by measuring the velocity, intensity, and magnetic field in the photosphere. Though measured at the Sun's surface, the oscillations propagate throughout the interior. Figure 1 shows two examples of internal wave propagation. The higher-ℓ p mode in the left panel is confined to a region near the surface, within the convection zone, while the other penetrates deeply, close to the core.

Non-radial acoustic waves are confined within a spherical shell inside the Sun by upward refraction due to the gradient in sound speed, c, and by downward reflection from the high density gradient just below the photosphere. The radius, r_1, of the central sphere of avoidance depends only on the frequency, ν, and the spherical harmonic degree, ℓ. The radius, r_2, where the waves are reflected downwards is essentially a function of ν alone, and is so close to the surface that the difference is not discernible in the figure. The eigenfrequencies of acoustic modes depend on the extent of the cavity within which they are confined and on the sound speed within that cavity. Thus, acoustic modes provide average information about c between r_1 and r_2, the average being weighted by the relative time spent by a wave propagating through a given region, which is proportional to c^{-1}. By combining information from two modes with slightly different values of r_1 but the same value of r_2, one can infer conditions in the small interval between the two values of r_1. This is a highly simplified illustration of the principle of inversion, the extraction of localized information from the global oscillations.

Conditions at some radius, r, are best inferred from modes whose lower turning points are close to r. For example, to resolve conditions at the 10,000

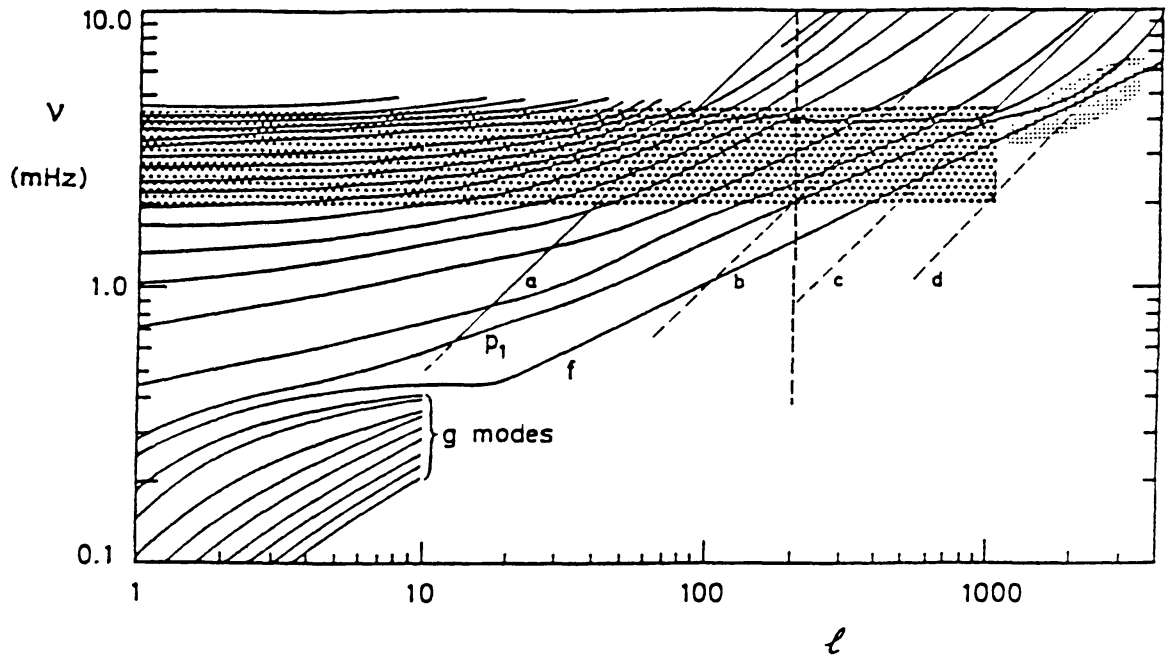

Fig. 2. The continuous curves show the frequency versus degree of the f, p_1, g_1, and higher even-order p and g modes for a standard solar model. MDI is sensitive to the signals anywhere in the diagram; ground-based observations have been limited to the rectangular shaded region. See text for details.

km - 20,000 km depth of the He II ionization region, which is necessary for determining the helium abundance, modes with $\ell \sim 300$ are required. Even higher-degree modes are required for investigating the vertical structure of supergranulation.

The regions in the solar interior that can be probed by modes of degree, ℓ, and frequency, ν, can be described using an $\ell - \nu$ diagnostic diagram. Figure 2 is a schematic representation of an $\ell - \nu$ diagram of trapped solar oscillation modes (at high ℓ this is equivalent to a $k - \omega$ diagram of horizontal wavenumber, k, and angular frequency, ω). The oscillations accessible to MDI include the whole diagram. The continuous curves are the frequencies versus degree of g_1, p_1 and the higher even-order p and g modes for a standard solar model. Odd order modes, except $n = 1$, were omitted for simplicity.

The intermediate- and high-degree p modes with 3- to 15-minute periods are the primary helioseismological probes of the interior dynamics. The heavy shaded region indicates where ground-based observations have been most successful. GONG is most sensitive to modes to the left of the vertical dashed line at $\ell = 200$. The four thin oblique straight lines marked a, b, c, and d indicate the p modes whose lower turning points are respectively at the base of the convection zone, the middle of the He II and H ionization zones, and the peak in the superadiabatic temperature gradient in the up-

per convective boundary layer. These lines are extended (dashed) beneath p_1 for clarity. The modes that are confined to the convection zone provide key information about the presumed large-scale motions that drive the solar cycle. The light shaded region is the region of greatest power detected by the Solar Optical Universal Polarimeter (SOUP) on Spacelab-II (Title *et al.*, 1989). There are no lines in the upper left corner of the diagram because those frequencies are above the Lamb acoustic cutoff ν_c, so the modes are not trapped. However, there are acoustic waves observed in this region that provide useful information about the depth of the acoustic wave source region (Kumar *et al.*, 1990; Kumar & Lu, 1991).

At high ℓ, frequencies of trapped modes can exceed ν_c because the modes are reflected by the corona. These modes provide information about the structure of the chromosphere.

Low-degree p modes with periods shorter than 15 minutes have been measured from the ground since about 1978 and were the first to be recognized as truly global modes (Claverie *et al.*, 1979; Grec, Fossat, & Pomerantz, 1980). Their frequencies give information on the gross structure of the Sun and are now a target for asteroseismology investigations of other stars.

Low-degree modes of intermediate frequency, 15 to 60 minutes in period, though likely only to be excited to very low amplitudes, may be detected by MDI. These modes are probably very long-lived and some should penetrate into the solar core. They have yet to be definitively detected.

The lowest frequency modes are the internal g modes, buoyancy modes trapped beneath the convection zone. Internal g modes are indicated in Figure 2 only for $\ell \leq 10$, because modes of higher degree are unlikely to be detectable (Appourchaux & Andersen, 1990). G modes have not yet been definitively observed. Because gravity modes provide the most sensitive measure of conditions in the solar core, the addition of only a few g-mode frequencies to the acoustic spectrum would significantly improve the precision with which the structure of the solar interior could be inferred. Knowledge of the frequencies of g modes of degree up to about 10 would provide limited latitudinal resolution of the energy-generating core. Gravity modes are also directly sensitive to the density gradient, and are thus likely to be an indicator of the smoothing of that gradient by overshooting at the base of the convection zone. This provides information about the extent of entropy mixing, vital to progress on the still unresolved problem of the depletion of lithium and beryllium in the Sun and other late-type stars. While the MDI instrument was not optimized for detection of very long-period oscillations, their detection is a goal of SOI.

2.2. Opportunities for Helioseismology

As the field of helioseismology has developed, several classes of instrumentation have evolved. Each has advantages for certain domains of phenomena,

characterized by the required spatial or temporal resolution, and the target region within the Sun. We briefly describe these domains, and SOI's contribution to each, below. MDI's three helioseismology observing programs fit into at least three of the domains: the Structure Program furnishes continuous coverage of solar features with low and moderate spatial frequencies, the Dynamics Program provides extended temporal coverage with intermediate spatial resolution, and Campaigns give higher spatial resolution for shorter intervals. These observing programs correspond to the telemetry opportunities available to MDI and are described in Section 5. For comparison, some of the other major helioseismology observing projects are also mentioned below. Of course, the scientific goals are not exclusive and will be achieved across these groupings.

Low-degree, long-period, continuous, very long-duration observations: Experiments like these measure slow variations of mode frequencies as the resonant solar cavity is affected by variations in levels of activity. They also observe low degree rotational splitting and possibly detect g modes. Examples include the BISON and IRIS networks. SOI will help in the calibration of these results and in interpreting the effects of solar activity on these measurements.

Low-degree, long-period, continuous, distortionless observations: These observations should be able to resolve low-degree rotational splitting and have the best chance of detecting g modes. They provide data on the deep interior including the energy-generating core. Examples include the MDI Structure Program, Phobos/IPHIR, SOHO/GOLF, and SOHO/VIRGO. SOI will also analyze specific Structure Program observations for use in collaborative studies with VIRGO and GOLF.

Intermediate-degree, continuous, long-duration observations: Modes of intermediate degree measure most of the solar interior, including most of the convection zone. They probe the stratification and large-scale features of internal rotation and can detect changes in the interior during the solar cycle. Continuous MDI Structure Program observations and GONG are presently the only programs that will measure these modes with continuity for long intervals. The MDI Dynamics Program will also contribute, providing up to two months of higher spatial resolution continuous coverage.

Intermediate- to high-degree, sets of partial day observations: These observations yield information about mode excitation, interactions with activity, and local dynamics. Analysis of these types of observations has resulted in the development of most of the techniques that will be exploited with GONG and MDI data. Examples include MDI Campaign Programs, subsets of the MDI dynamics data, Mt. Wilson Magneto-Optical Filter, NSO High-ℓ Helioseismometer, South Pole, and Big Bear Solar Observatory observations.

High-degree, continuous, distortionless observations: MDI is the unique example of an instrument that measures intermediate through very high de-

gree oscillations without atmospheric distortions for intervals long compared to mode lifetimes. The 2-month continuous high- rate telemetry Dynamics Programs will provide a unique opportunity to probe the convection zone in detail.

2.3. SOI Science Objectives

The primary scientific objective of the Solar Oscillations Investigation is to measure the internal stratification and dynamics of the Sun using the techniques of helioseismology. Not only will this provide information about the interior conditions that lead to the development of solar activity and the solar cycle, it will also impose stringent constraints on theories of stellar structure and evolution.

MDI will also make related, non-helioseismic measurements that are essential for understanding solar dynamics. Some of the related science goals can be accomplished with alternate analyses of the helioseismology data, but others will require different observations. MDI will make high-resolution and full-disk observations of line-of-sight velocity, line-of-sight magnetic field, line intensity, continuum intensity, and high-resolution transverse velocity. Descriptions of some of the helioseismology and related goals follow. The process for developing SOI science investigations is described in Section 6.

2.3.1. Convection Zone Dynamics

MDI provides four complementary views of giant cells and supergranulation. High-degree oscillations probe flow fields and thermal structures over a range of depths, especially within the zone of highly unstable stratification imposed by the H and He ionizations. The seismic results will be augmented by direct Doppler measurements of persistent, large-scale velocities in the surface layers and by horizontal velocities obtained from correlation tracking of intensity images. Maps of the magnetic network will provide cell geometries of supergranulation and larger-scale convection. Stellar theoreticians commonly assume that convection zone structure in stars is determined locally by small-scale turbulence. Yet the evidence on strongly nonlinear convection indicates a considerable degree of large-scale coherence, with cells extending from top to bottom of the zone and sometimes spanning a substantial range of latitude or longitude (Spruit, Nordlund, & Title, 1990). Local distortions of high-degree modes, measured in several ways, will permit mapping of the structure of individual giant convection cells. Mid-latitude jets have been suggested by some fluid dynamicists; accurate seismic monitoring is the only tool available for probing such motions below the surface.

Convection theory suggests that an effect of the rapidly decreasing scale height within the ionization zones is deflection of the largest-scale convective flows as they ascend, generating strong horizontal motions below the surface. The peak amplitudes attained within the shearing flows are uncertain, for

they depend sensitively on the rate of momentum braking. Modeling suggests that flows of 30 m/s near the base of the convection zone would lead to flow speeds ten times greater in the He II ionization region. MDI high-ℓ data should permit detection of horizontal flows with amplitudes of order 10 m/s.

2.3.2. Mean Radial Structure

The spherically symmetric component of the stratification of the Sun can be determined by inverting the mode frequencies averaged over all values of m at fixed n and ℓ. The results will permit us to test models of the distribution of density, pressure, and sound speed from the center to the solar surface.

The mean frequencies will allow us to determine the helium abundance, Y, in the outer convection zone of the Sun. Stellar evolution theory predicts that there has been no substantial contamination of the convection zone by the products of the nuclear reactions in the solar core; thus the value of Y in the convection zone should reflect the primordial solar abundance. The primordial helium abundance is a very important constraint on cosmological theories. We should also be able to infer $Y(r)$ in the inner radiative regions where nuclear reactions have taken place. This determines the nuclear age of the Sun, its temperature history, and whether mixing has occurred in the core. These data have important consequences for the theories of stellar structure and of main sequence evolution, and for cosmogony, as well as the neutrino problem.

Knowledge of the stratification is vital to two outstanding problems of solar/stellar structure: the equation of state in the convection zone and the opacity and thermal energy balance. Issues such as the degree to which bound-state energy levels of hydrogen and helium are shifted by electrostatic interactions with neighboring ions appear to have measurable consequences. Thus we anticipate being able to test theories of dense plasmas under conditions not attainable on Earth, and to improve calculations of opacity and the equation of state. We will be able to determine whether the thermal energy equations, using the modern opacity data, are satisfied in the radiative interior. If they are not, we must conclude that either the opacity has been incorrectly calculated or that the Sun is not in thermal balance. To differentiate between those alternatives will require studying the aspherical component of the stratification, determined from the symmetrical component of the degeneracy splitting of the oscillation eigenfrequencies.

2.3.3. Internal Rotation

The antisymmetric component of the degeneracy splitting of the wide range of acoustic and gravity modes accessible to MDI will let us determine the angular velocity Ω throughout the solar interior.

Knowledge of Ω is important to our understanding of the internal dynamics of the Sun, including the origin of the solar cycle. It is generally

believed that the solar cycle results from the interactions of convection, differential rotation, and the magnetic field. Helioseismic measurements of the rotation rate in the solar convection zone have indicated that the rotation rate is constant on radii, in sharp contrast to the constancy on cylinders expected from some numerical models. This would also suggest that any solar dynamo is likely to operate at the base of the convection zone. It is therefore extremely important to further constrain the rotation rate using helioseismic measurements.

Is the deep solar interior invariant over timescales of decades or centuries, or does it change with time, perhaps partaking in the solar cycle? An unstable angular-velocity configuration would imply that the structure of the hydrostatically stable solar interior beneath the convection zone must be time-dependent, with dynamical implications for the generation of meridional velocity and the transport of material through the energy-generating core. Additional evidence for that would come from the detection of a deviation from spherical symmetry of the mean structure (in addition to the asphericities associated with the solar rotation and surface effects). It would influence our computations of the time a star spends on the main sequence, and thus our estimates of the ages of globular clusters and of the galaxy.

Together with a knowledge of the hydrostatic stratification, the knowledge of Ω will permit us to compute the centrifugal distortion of the mass distribution, and hence obtain the quadrupole and higher moments of the external gravitational field with an accuracy much greater than is possible from tracking a spacecraft in an orbit passing close to the Sun. These moments must be accurately determined to test general relativity and other theories of gravity by the precession of planetary orbits.

2.3.4. Solar Core

The g-mode oscillations that penetrate to the energy-generating solar core have periods of several hours. In this range of periods MDI should be able to detect coherent oscillations of amplitude 1 mm/s with a signal-to-noise ratio (SNR) of about 5. If the mode energy is a function of frequency alone, as it is for p modes, then modes of degree up to about 10 might be detectable (Appourchaux & Andersen, 1990). The spatially unresolved measurements of GOLF will detect only modes with $\ell \leq 3$, because of the rapid decrease in sensitivity with increasing ℓ. The VIRGO experiment is the prime instrument for detecting g modes of higher order. Even with so few values of ℓ, the frequency spectrum is so dense in the g-mode range that it will be difficult to identify the modes without supplementary spatially resolved information from MDI.

Seismic diagnosis of the stratification in the radiative interior will provide important information about conditions in the core where thermonuclear reactions take place. Although GONG will also be concerned with this issue,

the high-degree modes accessible only to MDI are essential for resolving basic uncertainties in the structure near the photosphere where all p modes are reflected. With data from MDI, GOLF, and VIRGO, we can determine the temperature of the core where neutrinos are produced. This will reduce the uncertainty of the count rates predicted for the various neutrino experiments. Likewise, information obtained from g modes will help establish whether large-scale circulation transfers angular momentum and nuclear reaction products out of the core, issues of importance in understanding why the bulk of the radiative zone rotates more slowly than the convection zone.

2.3.5. Magnetic Structures and Activity Cycle

Helioseismic probing of the solar magnetic field received relatively little attention until recently, because models assuming a uniform field predict immeasurably small effects. However, if an equivalent magnetic flux is concentrated in flux tubes with filling factor, f, it produces a frequency shift larger by f^{-1}. Since f is, in fact, very small in the photosphere, magnetic effects are greatly enhanced. The largest frequency shifts are expected to occur for high-ℓ modes localized near the solar surface. The predicted frequency shifts are at the 0.1% level, and can be measured by MDI in several days of continuous coverage.

It has been shown that sunspots act as absorbers for high-ℓ p modes (e.g., Braun *et al.*, 1988). The high-resolution mode of MDI will be used to study the modification of solar oscillations by sunspots and active regions. The p-mode scattering amplitudes will provide diagnostics of the formation process and sub-surface structure of active regions. This will allow calibration of the magnetic influences on the p-mode spectrum, so that the structure inferred from inversions will not be distorted by magnetic field effects. We will also search for intense internal magnetic fields, such as concentrated bands in the radiative interior or at the base of the convection zone. The seismic diagnosis should shed light on the large-scale flows in the convection zone that are responsible for the field reversals, butterfly diagrams of magnetic activity, and torsional oscillations associated with the solar cycle.

2.3.6. Excitation and Damping

So far, the discussion has been restricted to inferences that can be made from mode eigenfrequencies alone. However, mode phases and amplitudes also contain useful information. The phase relation of intensity and velocity in the photosphere is determined by the interaction of the oscillations with radiative transfer in the solar atmosphere and by the dynamical modulation of turbulent transport in the convection zone. The former can be studied by measuring the variation of oscillation amplitudes with height in the atmosphere. For long-period modes, the atmosphere has too small a heat capacity to store sufficient energy to modulate its phase, and must

simply adjust itself to pass whatever flux is provided by the convection zone. Consequently, phase studies provide extremely valuable data for evaluating theories of time-dependent convection. This is of great interest for modeling variable stars such as the redder Cepheids, RR Lyrae stars, long-period variables, and DA white dwarfs.

The interaction between convection and the oscillations also influences the amplitudes of the modes. Short time-scale variations determine the widths and asymmetries of individual modes in the frequency spectrum. Long time-scale variations can be measured directly to study the growth and decay of modes and the nonlinear energy exchange between them. Currently, such data can be used only to test theories of mode excitation and scattering, but with theoretical advances we anticipate inverting the data to measure the statistical properties of turbulence in the convection zone.

2.3.7. Convection and Large-Scale Flows

MDI is uniquely suited to the task of detecting and monitoring the convective flows in the photosphere that have so far remained elusive to ground-based observations. The smaller-scale components of this flow, mesogranulation and supergranulation, are difficult to follow because their line-of-sight velocity is small except near the limb; while large-scale motions such as giant cells and meridional flows are hard to detect because they only have velocities of $\sim$ 20 m/s or less. Reliable identification of these flows can best be achieved by simultaneous measurements of the line-of-sight velocity and the transverse velocity inferred from correlation tracking of small-scale features. Continuous measurements lasting eight hours will be sufficient for identification and confirmation of large-scale flows and will yield some data on the evolution of mesogranulation. Studies of the development of active regions and the evolution of supergranulation will be the targets for extended campaigns lasting several days.

2.3.8. Magnetic Field Measurements

Magnetic fields are of fundamental importance in the physics of the Sun. Flux tubes, coronal holes, energetic flares, and the 11-year solar cycle all depend on the configuration and dynamics of the field. MDI obtains high-quality synoptic observations of the full-disk line-of-sight magnetic field, free from atmospheric distortions, every 96 minutes. These measurements will be interleaved with the primary helioseismology observations to produce minimal impact.

Doppler observations, and therefore oscillation measurements, are significantly contaminated by the effects of strong magnetic fields on the line profile. Magnetic field information is also important because strong fields modify physical conditions sufficiently to affect the p-mode spectrum. Effects include direct scattering and absorption of acoustic waves as well as

alteration of the turbulence spectrum, as evidenced by significant changes in the scale and lifetime of convective cells of all sizes. Fields are also associated with large-scale motions in the surrounding region. MDI will provide data to evaluate and allow for such effects on the oscillations.

2.3.9. Magnetic Diffusion and Field Advection

Because measurements of the magnetic field only reveal the configuration at the solar surface, critical gaps exist in our understanding of the formation of sunspots, the formation and dissolution of active regions, and the magnetic geometry leading to coronal mass ejections and possibly flares. Subsurface flow fields determine the field location. With precise measurements of the magnetic field and the flow fields below the surface, we will be able to better understand the mechanisms of active region development. Conversely, by mapping the field and its evolution we will be able to confirm the subsurface flows inferred from seismology with an independent tracer.

We expect that the Dynamics Program data will reveal the subsurface geometry of giant cells, meridional currents, supergranulation, and mesogranulation cells. Local correlation tracking of the same images will measure the horizontal flow fields associated with the cells at the surface. Interspersed magnetic maps will show how the fields are arranged on the cell boundaries. Together these three types of measurements will help to form a complete picture of the magnetic evolution at the surface.

Full-disk synoptic magnetic observations taken about 15 times per day provide superior coverage to ground-based observations because of their cadence, uniformity, and freedom from distortion. They will allow study of the redistribution of field elements over the solar surface. MDI magnetograms will allow determination of the local magnetic diffusion coefficients, with even higher time resolution during special campaigns. Comparison with diffusion coefficients estimated from measured sizes and lifetimes of supergranulation cells will directly confirm or contradict models of solar flux dispersal. SOI will also determine the role of large-scale flows in field redistribution.

2.3.10. Limb Figure Measurements

MDI will make the first photometric observations of the complete solar limb from above the atmosphere, determining the shape of the solar disk to an accuracy of about $0.0007''$ each minute. In addition to the shape measurement, precise brightness measurements of the solar limb are of great interest. Previous observations of solar latitude-dependent limb brightness variations, equivalent to a latitudinal temperature variation of approximately 1 K, are the signature of large-scale meridional circulation (Kuhn, Libbrecht, & Dicke, 1988). Because of limb-darkening, brightness variations are tied to shape measurements, so both must be observed simultaneously. Dynamic

variations in the shape and limb brightness are a sensitive measure of low frequency p and g modes.

2.3.11. Radiative Flux Budget

MDI makes medium-resolution proxy measurements of continuum brightness and of magnetic region coverage. These observations, in collaboration with VIRGO and ground-based programs, will allow a determination of their relative contributions to variations in total irradiance.

3. The Michelson Doppler Imager Instrument

MDI is based on a modification of the Fourier Tachometer technique (Brown, 1980; Evans, 1980). MDI uses a refracting telescope to feed sunlight through a cascade of filters onto a CCD camera. Two tunable Michelson interferometers (Title and Ramsey, 1980) define a 94 mÅ bandpass that can be tuned across the Ni I 6768 Å solar absorption line. Velocity, continuum intensity, and other observables are computed on board from combinations of filtergrams, as described in Section 4.

The MDI instrument consists of two physical enclosures: the optics package (OP) and the electronics package (EP). The OP contains all of the optics: the telescope, the image stabilization system, spectral and polarizing filters, the beam distribution system, the shutter, and the CCD camera, as well as noise sensitive electronics. The EP houses the circuit boards for instrument control and communications, the image processor with over 42 MB of memory, and the power supplies. The OP and EP are connected by shielded cables. The OP is isostatically mounted to the spacecraft on six legs. The pointing of the OP can be adjusted after launch using an alignment mechanism on the back legs. A front door protects the optics during launch. Figure 3 shows the OP without its lid.

The internal elements are labeled in Figure 4, which shows a schematic of MDI's light path and the primary optical components. The green-colored portion identifies the telescope, filter wheels and Image Stabilization System (ISS). Retarders in the polarization analyzer wheel convert the right or left circularly polarized component or the vertically or horizontally polarized component of the incoming beam into vertically polarized light. The ISS beamsplitter sends that component through the instrument while reflecting the orthogonal component onto the bi-cell limb sensors.

The two calibration/focus wheels contain variable thicknesses of glass in three positions that can focus the image over a range of nine depths of field. A pair of lenses in the fourth position of each wheel images the pupil onto the focal plane for calibration purposes.

A very precisely controlled oven (contents coded blue) houses all of the filters (except for the 50 Å front window) as well as the reimaging optics. The

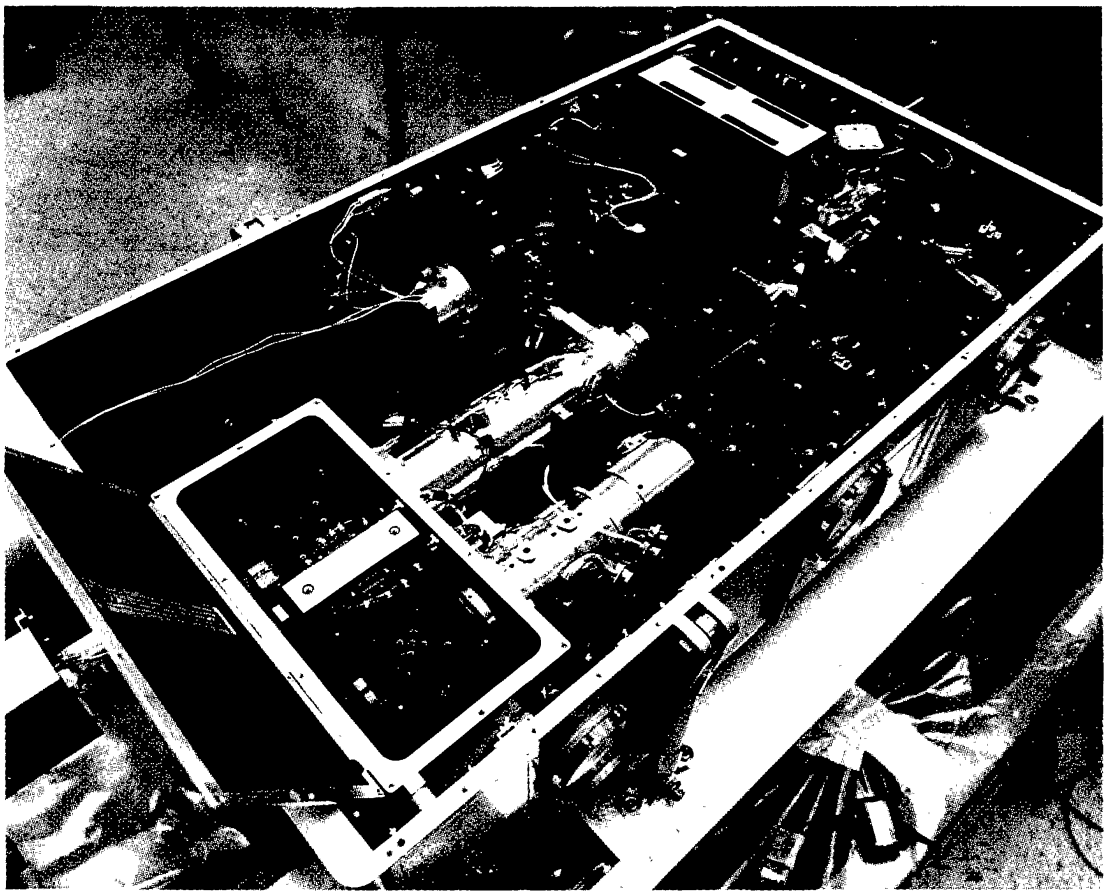

Fig. 3. Photograph of the Optics Package (OP). The top cover is removed to expose the major components. The oven and the beam distribution system also have their covers lifted. The Michelson interferometers with both tuning motors mounted between them are visible in the oven. One of the fiberglass mounting legs is visible on the side of the OP.

blocking filter is 8 Å wide and the Lyot FWHM is 465 mÅ. The Michelsons, FWHM of 188 mÅ and 94 mÅ, are tuned with rotating waveplates. A lens makes the beam telecentric through the filter system, i.e., the angular distribution of light passing through the filters is identical for each image point.

The contents of the beam distribution system and the CCD camera are shaded red. MDI can observe in either of two spatial resolutions, as selected by the shutter. The full disk (FD) path has a field of view of 34x34′ with 4″ resolution. The high-resolution (HR) path is magnified by a factor of 3.2 to provide 1.25″ resolution over an 11′×11′ field of view. The detector system employs a passively cooled 1024×1024 CCD that is read out at 500,000 pixels per second.

The MDI instrument is described below as six interrelated subsystems: Imaging and Mode Selection Optics, Pointing and Image Stabilization, Filter System, Camera System, On-board Control and Image Processing System,

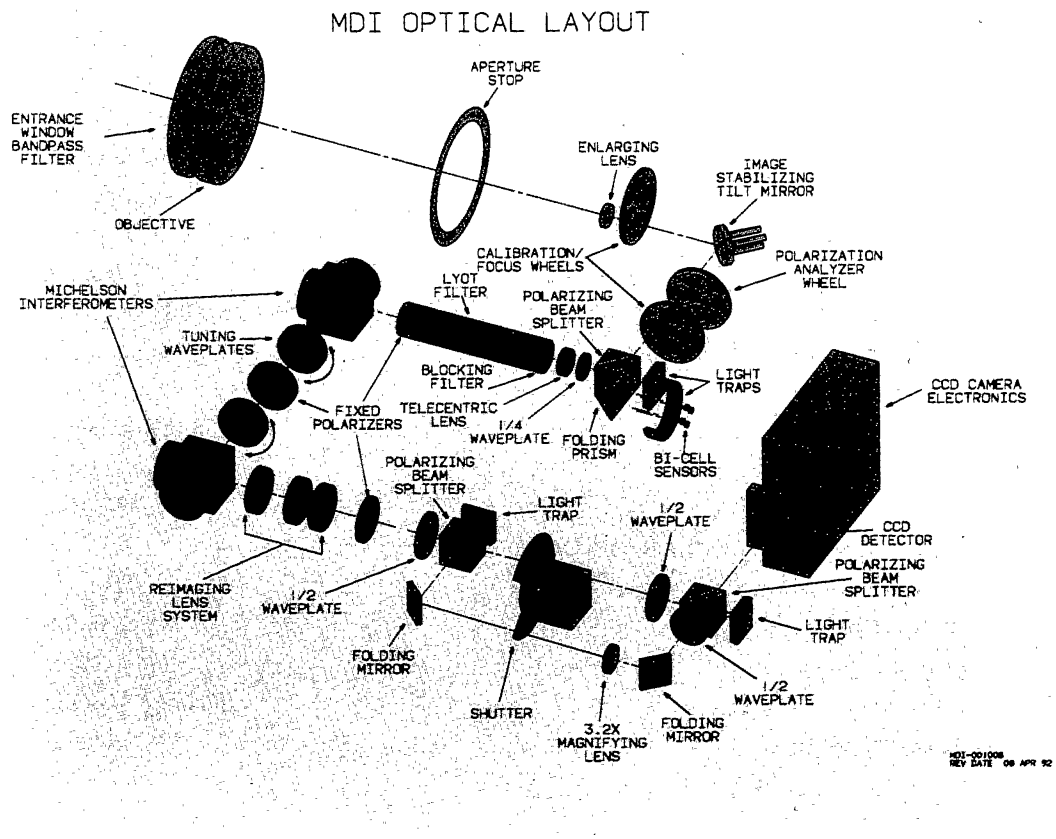

Fig. 4. Schematic of MDI's Optical Layout, see text for description.

and Mechanisms. Table I summarizes some key parameters of the instrument.

3.1. Imaging Optics

This section describes the optical components of MDI. Every glass-vacuum interface is anti-reflection coated with very high efficiency at 6768 Å.

The 12.5 cm primary (objective) and the secondary (enlarging) lens form a telescope with an effective focal length of 1867 mm. The light is folded by the ISS mirror and then split by a polarizing beamsplitter/prism to project two primary images. The p-component guiding image falls on the limb sensor assembly of the ISS. The s-component primary image plane lies a short distance inside the filter oven. A quarter-wave plate mounted between the beamsplitter and the oven directs undesired reflections from the filters back through the beamsplitter onto a light-trap. This circularly polarizes the light in the observing beam, so only half the light passes through the linear entrance polarizer of the Lyot filter.

TABLE I
Key Parameters of MDI

Telescope Aperture	12.5 cm
Focal Plane Array	1024 x 1024 21μm pixel CCD
Resolution	4″ (FD) and 1.2″ (HR)
FOV Full Disk	34 × 34 arcmin
FOV High Resolution	10.5 × 10.5 arcmin
Spectral Range	6767.8Å ± 190mÅ
Spectral Bandwidth	94mÅ
Selectable Polarizations	S-wave, P-wave, RCP, LCP
Temporal Resolution (cadence)	3 seconds
Pointing Stability	0.02″
Off-pointing Range	13 arcmin
Maximum ℓ of modes	4000
Maximum Mode Frequency	17 mHz
Noise Performance (per pixel in 1 minute)	
Doppler Velocity	20 m/s
Continuum Intensity	0.3%
Magnetic Field	20G
Mass	56.5 kg (total)
Optics Package	23.8 kg
Electronics Package	31.0 kg
Cables	1.7 kg
Power	38 W
Science Telemetry	5 kbps (continuous)
	160 kbps (high-rate)

The lens that serves as the entrance window of the oven images the pupil to infinity. This produces a telecentric beam for the subsequent filters. A set of lenses at the exit of the oven reimages the primary focus onto the detector. An image of the pupil is located close to the shutter near the exit from the first beamsplitter in the beam distribution system.

The beamsplitters and folding mirrors in the beam distribution system separate the FD and HR paths. The FD pixel size of 2″ would result in aliasing due to undersampling of resolved spatial structures, so to minimize this effect the FD path is defocused by two focus steps. This decreases the Modulation Transfer Function (MTF) from 47% to 17% at 80% of the Nyquist frequency in the FD path, while reducing the MTF of the aliased signal from 22% to 3%, compared to the uncorrected case.

The Barlow lens in the HR path magnifies the image by 3.2. The intensity ratio of the beams is 14:1 (HR:FD) to provide comparable exposure times

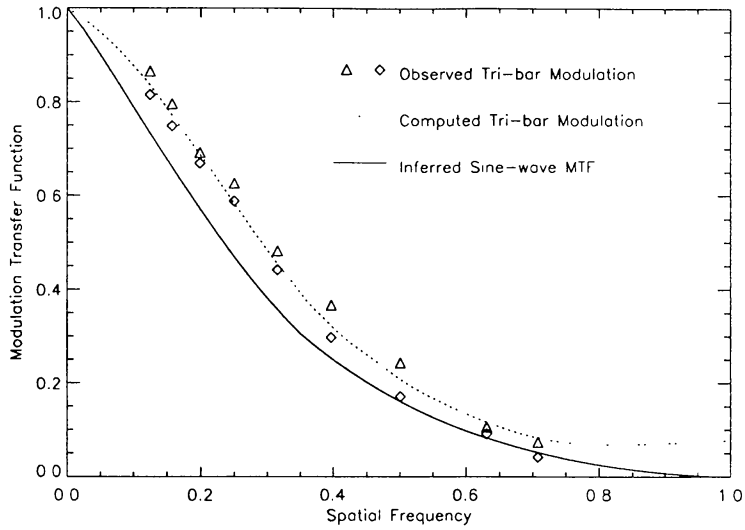

Fig. 5. The square-wave Modulation Transfer Function (MTF) measured from a tri-bar target in the HR path (center of field of view). The dashed curve is a fit to the measurements; the solid curve is the sine-wave MTF inferred from it.

for the two paths. The shutter selects which beam falls on the CCD. The HR field of view is centered on the solar central meridian, but offset towards the northern hemisphere by 160″ to allow observation of active regions. The resolution of the telescope and CCD are matched in the HR path, where the pixel size corresponds to 0.625″. In high-resolution mode MDI achieves near diffraction-limited resolution. Figure 5 shows the measured square-wave MTF for the center field of view. The relation between sine-wave and square-wave MTF has been derived empirically and fit to the measured points. The inferred sine-wave MTF (from the one parameter fit) is plotted as the solid line: it is consistent with the theoretical sine-wave MTF using expected values for diffraction, random wave-front error, jitter, and the discrete sampling. The fit beyond approximately 0.7 of the Nyquist frequency may not be unique.

For normal observing (OBSMODE), nine possible combinations of glass plates (three in each calibration/focus wheel) can adjust the focus of the primary image over a range of nine depths of field. The optics have been adjusted to place the proper focus for both the FD and HR paths in the middle of the range at launch.

A fixed optical distortion does not effect Doppler measurements; however, it does generate errors in transverse velocities determined by correlation tracking. The measured distortion of 0.25% peak-peak over the entire FD field of view will produce a velocity error less than the 20 m/s Doppler velocity error.

For calibration it is desirable to have an identical input signal at each pixel. Since the CCD focal plane is the image of the primary focus image,

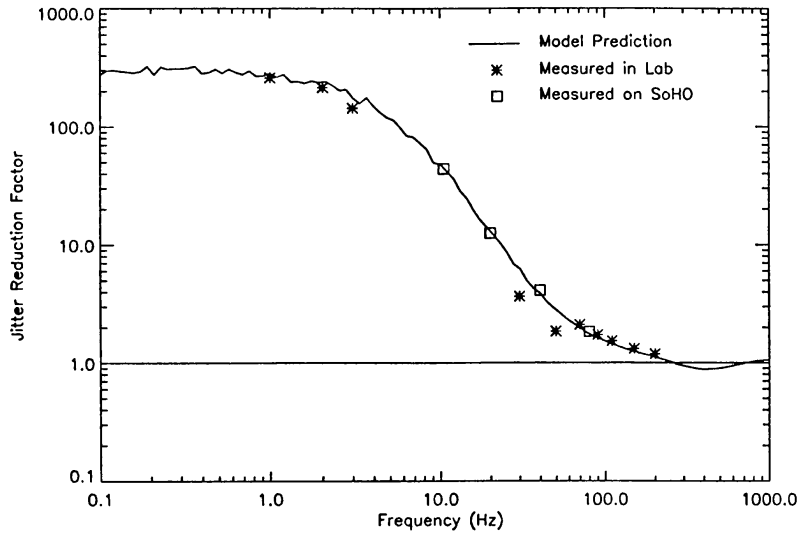

Fig. 6. Servo response curve of the ISS. The solid curve represents the theoretically predicted response, while the symbols show measurements in several frequency domains in the laboratory and after mounting on the SOHO spacecraft.

this is accomplished by forming an image of the pupil at the prime focus. To select calibration mode (CALMODE), the first calibration/focus wheel positions a lens immediately behind the secondary lens to cancel its effect, while a lens in the other calibration/focus wheel images the telescope's pupil onto the primary focal plane. This brings the front window and the objective nearly into focus and provides integrated sunlight to the detector.

3.2. The Pointing and Image Stabilization System

The ISS is a closed loop servo control system that uses the image of the solar limb projected onto four orthogonal detectors at the guiding image focal plane. Each detector consists of a redundant photodiode pair. The system uses a 3-point piezoelectric transducer (PZT) actuated mirror to remove errors in the observed limb position. The total tilt range of the active mirror is $\pm 19''$ while the operational jitter range is $\pm 7''$. Figure 6 shows the predicted and measured ISS servo response curve for nominal gain.

Jitter of photospheric features results in intensity fluctuations that translate into velocity errors. The specification for MDI's ISS derives from the stability required for a 60-second velocity measurement. The jitter must be reduced to less than $0.03''$ peak-to-peak, a twentieth of an HR pixel, to keep the velocity error below 7 m/s.

The ISS provides for adjustment of several variables in the servo loop. In particular, offsets can be added to the X and Y axis error signals to change the nominal pointing while maintaining lock. The resolution for closed-loop offsets can be selected between about 0.2 and $0.1''$ per step; the actual values will depend on the system gain in halo orbit at L_1. In CALMODE the

ISS detectors are illuminated by the pupil image, so closed-loop operation is impossible and the mirror must be held fixed. Individual PZT actuator offsets can be specified to fix the nominal position of the mirror anywhere in its range during open loop operation or during special calibrations.

The error signals are continually sampled at 16 Hz, averaged over 7 seconds, and down-linked in the housekeeping channel to monitor jitter. For special calibrations the error signals will be sampled and down-linked at 512 Hz using the high-rate telemetry channel.

The alignment mechanism can adjust MDI's relative pointing over approximately 13′. The legs will be adjusted after launch to center the solar image on the CCD with the ISS mirror in its middle position. Electronic offsets will then be commanded to null the error signals, compensating for any misalignment between the CCD and the limb-sensors. Further operation of the alignment mechanism is not planned except for special calibrations and occasional corrections of pointing due to thermal distortions.

3.3. The Filter System

The heart of the MDI instrument is the filter system. The filter system enables narrow-band (94 mÅ) filtergrams to be made anywhere in the vicinity of the Ni I 6768 Å mid-photospheric absorption line. The system consists of the front window, the blocker, the Lyot, and two tunable Michelson interferometers. These elements define the instrument transmission profile. The fixed filters transmit light only near the Ni I 6768 Å line and have a combined FWHM of 454 mÅ. The Michelsons have sinusoidal bandpasses with periods of 377 mÅ and 189 mÅ. Filtergrams anywhere in the vicinity of the solar spectral line can be obtained by tuning the Michelsons' peak transmission. In normal operation filtergrams are obtained at five tuning positions 75 mÅ apart spanning the 377 mÅ tuning range. Figure 7 illustrates the situation where the solar line is sampled at two of these nominal wavelengths. The transmission profiles of the Lyot and Michelsons were designed to minimize intensity modulation from the background continuum. Measurements with a white-light source yield a peak-to-peak variation of few percent despite the apparent large sidelobes shown in the upper panels of Figure 7. Table II summarizes the filter properties as measured with a tunable laser and the Sun.

Doppler shift measurements of long period oscillations require a filter system with a very stable and reproducible passband. Both the Lyot filter and Michelson interferometers have temperature compensating designs, and all the filters, except the front window, are mounted in a highly stable oven.

The telecentric optical system ensures that each CCD pixel is illuminated by a cone of rays that has identical angular distributions through the narrow-band filter section. However, any variation in transmission efficiency over these cones will produce small variations in the integrated transmission

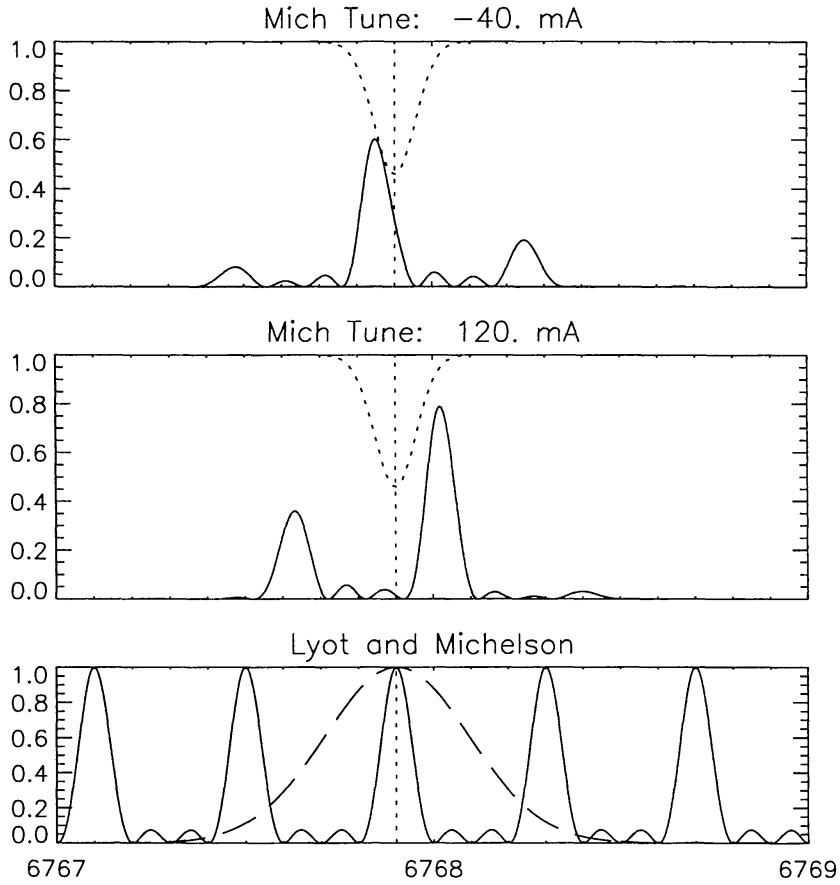

Fig. 7. MDI's principle of operation. The lower panel shows the individual profiles of the Lyot filter (dashed line) and the channel spectrum of both Michelsons in series (solid line). The upper panels illustrate the situation for two of the four nominal Doppler tunings. The solid line represents the resulting instrument transmission profile for the corresponding tuning position with respect to the 6768 Å line profile (dotted line).

profile for each pixel. Also, an important difference exists in the spectral properties of the cones of light between OBSMODE and CALMODE. In OBSMODE, the cone of rays for each pixel comes from a particular point on the Sun, so each ray has the same Doppler shift. The cone for each CCD pixel will have a unique Doppler shift due to variations across the solar surface. In contrast, each pixel in CALMODE sees the whole Sun, because it stems from a different point on the pupil. Thus every CALMODE cone has the same average Doppler shift. However, angular position in CALMODE cones map to location on the Sun. This mapping is the same for each CALMODE pixel, but the Doppler shift now varies across the cone itself. This is relevant for the calibration of velocity measurements discussed in Section 4, because angular and spatial filter non-uniformities produce different velocity errors in the two modes.

The front window, with a bandpass of 50 Å, is the first element of the filter system. It is a two-element bonded design, with a multilayer dielec-

TABLE II
Summary of Measured Filter Parameters

Parameter	Measured Value	
MICHELSONS	M1	M2
Free Spectral Range	189 mÅ	377 mÅ
Tuning Contrast	99 %	99 %
Non-uniformity (laser)	60 mÅ p-p	160 mÅ p-p
Non-uniformity (sunlight)	20 mÅ p-p	50 mÅ p-p
Angular Sensitivity	± 22 mÅ	± 28 mÅ
Temperature Sensitivity	-9 mÅ/°C	-14 mÅ/°C
LYOT		
Central Wavelength	45 mÅ red of mean solar wavelength	
Profile Shape	465 mÅ FWHM; 4 & 2 % side-lobes @ ± 2.7 Å	
Uniformity	25 mÅ p-p	
Angular Sensitivity	0 - 65 mÅ	
Temperature Sensitivity	≤ 8 mÅ/°C	

tric coating sandwiched between RG630 red and GG475 yellow glass plates, each having a thickness of 7.5 mm. The front window is the only blocker of infrared, to which the CCD is very sensitive. Four small pinholes in the infrared blocking layer are visible in CALMODE, that produce an excess brightness of 25% when observing through Earth's atmosphere. The areas are well localized in CALMODE and can be calibrated out. In OBSMODE the excess energy spreads out over the entire field of view and contributes less than 10^{-5} to each pixel because the pinholes are a tiny fraction of the entire aperture. The HR CALMODE field of view includes no pinholes.

The limb sensors receive the full 50 Å bandwidth, while light for the rest of the instrument continues through the 8 Å bandpass blocking filter located just inside the oven. The blocker is a three-period all-dielectric interference filter. In collimated light, the blocker transmission profile has a ripple of about 1%, which averages out to less than 0.1% for the telecentric f/14 beam and a period of 485mÅ. The ripple amplitude is reduced by a factor of 10 in OBSMODE and a factor of 7 in CALMODE. Uniformly distributed tiny imperfections in the blocker become visible in collimated light, but these "chicken pox" are completely attenuated in the f/14 beam. The temperature sensitivity of the blocker is 0.2 Å/K.

The fixed-wavelength, wide-field, temperature-compensated Lyot filter (Title & Rosenberg, 1981) has a bandwidth of 465 mÅ. The six-element Lyot, which is of 2:2:4:4:6:8 design, is assembled from more than 70 com-

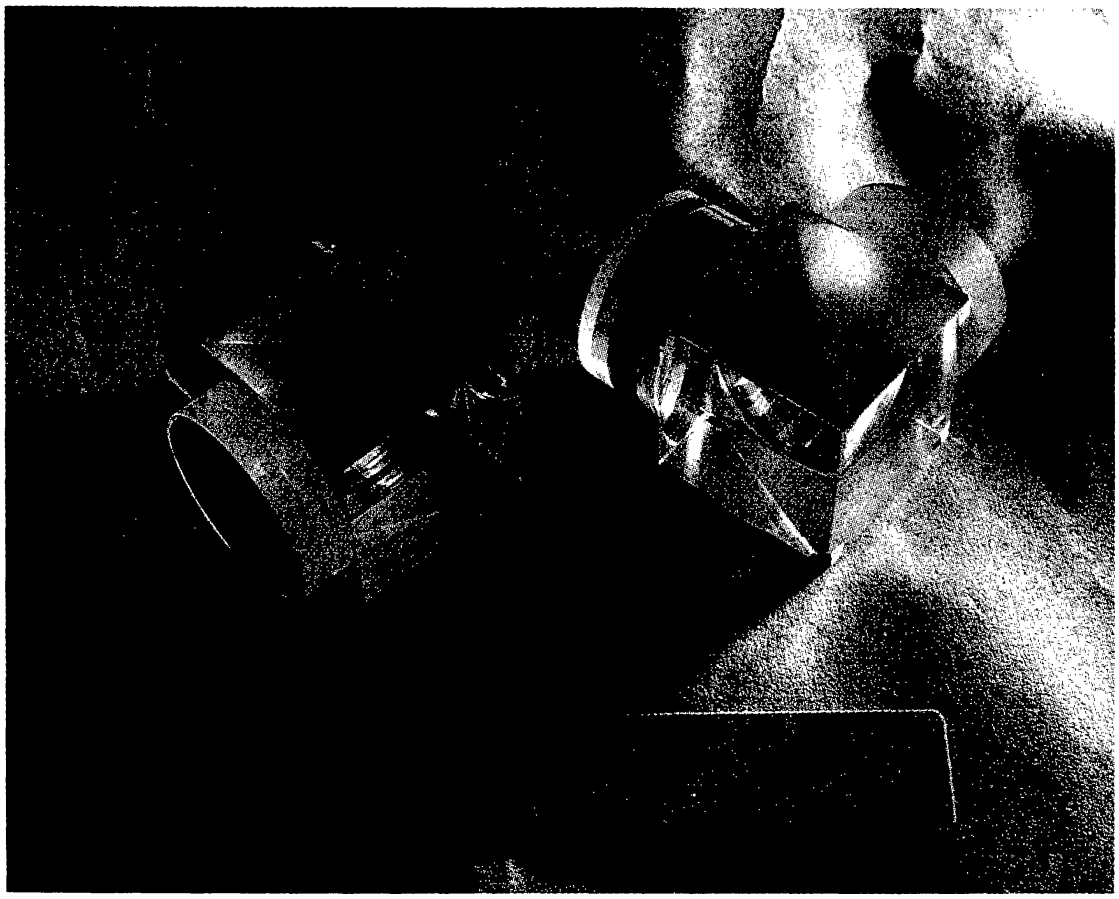

Fig. 8. Photograph of the flight Michelsons. Note the stress-reducing "Stonehenge" design of the copper standoffs in the vacuum leg. Kapton tape encloses the latter to maintain cleanliness.

ponents. The end caps are keyed and hold the elements in proper relative alignment. The components are not glued, but rather greased together using Dow Corning Q2-3067 couplant. The entire Lyot assembly, which is mounted in the tube of the filter oven, has a total length of 157.2mm. This includes the blocking filter, a 3.6mm glass slug to achieve the final focal length, and the exit polarizer. The Lyot has a measured temperature sensitivity of less than 8 mÅ/K. The Lyot (and the Michelsons) were calibrated in the instrument (cf. Table II).

The final spectral filters are a pair of tunable solid Michelson interferometers with a clear aperture of 43 mm and free spectral ranges of 189 mÅ and 377 mÅ. The design incorporates a polarizing beamsplitter of BK7 glass with a vacuum leg and a solid glass leg. The vacuum leg is maintained with temperature compensating copper standoffs. Figure 8 shows the flight Michelsons, which were built by Interoptics Ltd. The "Stonehenge" design

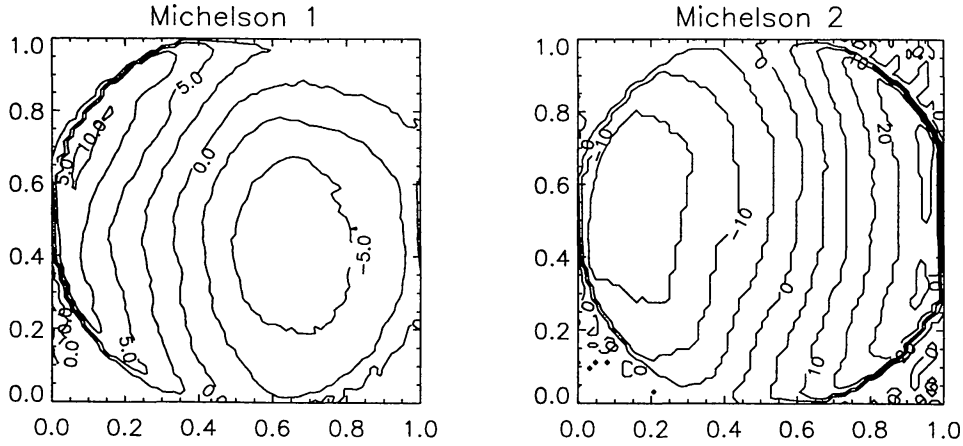

Fig. 9. Michelson central wavelength maps: spatial variation of the peak transmission wavelength for each Michelson from solar measurements in mÅ. M1 is the narrower interferometer.

of the copper spacers reduces stress in the glass. Tuning is accomplished by rotating half-wave retarders in the Michelson Tuning Motors (MTMs) mounted between the interferometers. MTM1 is mounted at the output of the 188 mÅ interferometer; MTM2 is at the input of the 94 mÅ Michelson.

For each filtergram the channel spectrum of each Michelson must be individually tuned for maximum transmission at the desired wavelength. Any image displacement between filtergrams (due to wedge in the rotating waveplates) will generate noise in the Doppler measurements. Measurements show that the images remain registered to within 0.15″ throughout a full rotation of either MTM. This is comparable to the image motion due to solar rotation in one minute. In high resolution this could cause a velocity error of up to 20 m/s.

Unfortunately, the central wavelength of the interferometers varies significantly across their faces, producing a difficult calibration problem. Thermal transient tests indicate that mechanical stresses in the vacuum-spaced interferometer legs are responsible for at least some of the non-uniformity. Maps of the peak transmission wavelength of each Michelson are shown in Figure 9. The narrow line width of a laser provides the ideal diagnostic tool, but measurements can also be made using solar illumination so that similar maps will be made routinely during the mission. The two methods generate somewhat different maps due to different spatial and angular averaging involving both instrument geometry and solar effects (limb darkening, rotation, center-to-limb variation of the line profile, etc.). Detailed simulations will determine how to best use the solar maps for Doppler calibrations during flight.

The filter oven that houses the temperature sensitive filters is mounted on a set of fiberglass legs that carry the mechanical loads and thermally isolate it from the OP. This provides a temperature stability of better than $\pm$ 0.01°C/hr. The Michelsons and Lyot are also mounted on fiberglass to further isolate them and increase stability. The operating temperature of the oven is selectable in 1° increments between 33 and 40°C and is of lesser importance than its stability. The OP itself is held stable to better than $\pm$ 0.5°C/hr at a temperature near 20°C using a system of heaters and passive radiators. It is mounted on fiberglass legs to minimize OP susceptibility to spacecraft fluctuations. As part of the overall thermal design, the front window's absorptivity/emissivity ratio (0.3) is tailored to operate near 20°C, minimizing thermal stresses in its mounting.

The polarization selection optics are part of the filter system. Waveplates in the polarization analyser wheel convert the desired input polarization (s-wave, p-wave, LCP or RCP) to vertical linear (s-wave) polarization. The s-component of the beam entering the ISS beamsplitter feeds the instrument, while the p-component feeds the ISS sensors. The waveplates themselves are virtually 100% efficient. However, oblique reflections cause some instrumental polarization. A remaining concern is the crosstalk between circular and linear polarization as this causes velocity measurement errors in magnetic regions.

For magnetic measurements the polarization analyser wheel moves between RCP and LCP positions between filtergrams. Any corresponding image displacements or distortions will cause erroneous magnetic signals. We have measured the differential distortion between RCP and LCP to be less than 0.4″ p-p over the FD field of view. The rigid displacement due to the waveplate wedge was measured to be less than 0.2″. Ideally, the ISS would correct this image motion, since the ISS sensors are after the polarization analyser wheel. However, even small differences in the intensity distributions of the RCP and LCP images will introduce an image displacement. The resulting small displacement will cause small systematic errors in FD magnetograms. The errors cannot be ignored in HR mode, so the images will be registered in the IP prior to computing the magnetograms.

Nominally, all Doppler measurements will be made in s-wave. The additional capability to observe in p-wave provides greater visibility into linear polarization effects on Doppler measurements.

3.4. Camera System

Development of a space-qualified CCD camera system was a major component of the SOI program. The camera consists of a CCD chip mounted in a header, a temperature/contamination control system, a radiation shield, and camera electronics.

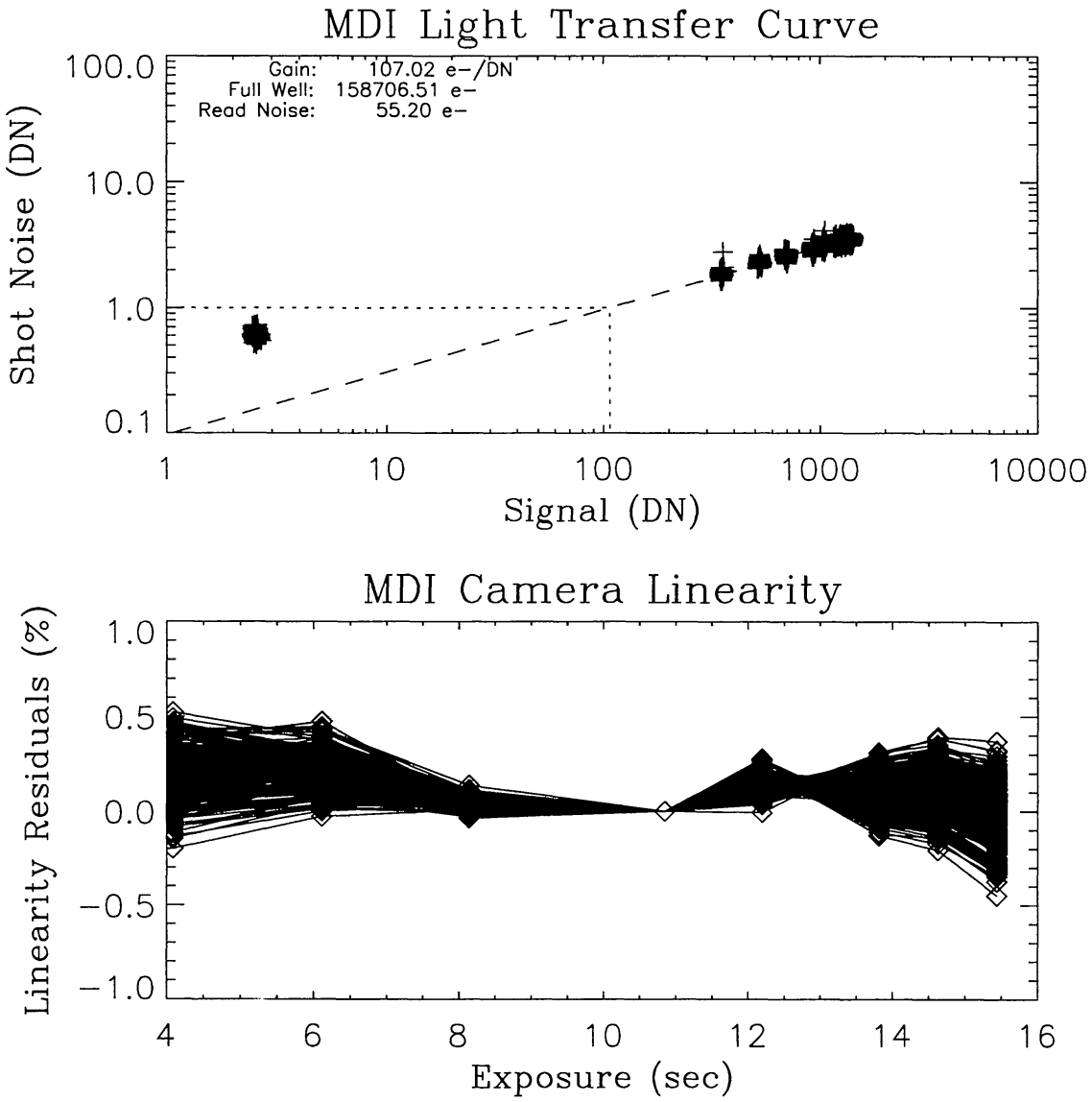

Fig. 10. Routine monitoring of CCD camera performance. The top panel shows the light transfer curve from which several parameters are derived. Linearity residuals are plotted in the bottom panel. Each data point is an average of a 16^2 pixel area within the central 256^2 portion of the CCD.

The CCD is a front-illuminated, 3-phase 1024×1024 array with 21 micron square pixels manufactured by Loral Aeroneutronic. It is an MPP technology device operated partially inverted to increase the full well capacity. Values for full well, read noise, dark current, system gain, relative charge transfer efficiency (CTE) and linearity are obtained from the routinely measured light transfer curve (see the top panel of Figure 10). The linearity residuals, calculated from 16^2 pixel averages within the central 256^2 portion of the CCD, are plotted in the bottom panel of Figure 10.

Low-signal absolute CTE calibration was obtained from Fe^{55} laboratory measurements which inject known amounts of charge (5.9 keV X-rays) into the device. The following values summarize the flight camera's performance at -70 °C: maximum signal: 450 ke^-; read noise: 50 e^-; dark current: 0.3 e^-/s; system gain: 110 e^-/DN; CTE: 0.999995 (1/2 full well), 0.99998 (Fe^{55}). Proton damage tests were carried out using LPARL's Van de Graaff accelerator on a flight-like CCD array and the expected end-of-mission CTE degradation was modeled (Zayer *et al.*, 1993). The results indicate that the CTE should stay above 0.9999 and will not degrade the MTF at the center of the array by more than 10% at half the Nyquist frequency.

The CCD is mounted onto a gold-flashed Elkonite (W-Cu alloy) header whose temperature coefficient approaches that of silicon. A copper thermal strap connects the header to a 960 cm^2 radiator that cools the detector to a nominal operating temperature near -80°C. The actual value will depend on the sink temperature at L_1. An open loop adjustable heater with a maximum input of 30 W is mounted on the header. The heater can boil off contaminants and provides the option of adjusting the operating temperature. To reduce radiation damage, mainly from medium-energy flare protons, an aluminum shield of at least 1 cm thickness surrounds the CCD.

The preamplifier stage is connected directly to the CCD's pins and runs at the same cold temperature, optimizing noise performance. The remaining camera electronics, running at about 25 °C in the OP, are connected to the preamplifier circuit board via a pair of low therma-conductance flex cables. The CCD is read out at 500 k pixels/s with 12 bit resolution. The system gain is adjusted such that the A/D converter reaches its saturation slightly before the CCD reaches its full well capacity. Each unit of digital signal corresponds to 110 photo electrons.

To avoid injection of noise, MDI will not actuate mechanisms during the 2.2 second camera readout. To maintain the required 3-second exposure cadence, the time available to reconfigure the instrument for the next exposure is 0.8 seconds minus the exposure time (nominally 100 ms). The CCD is in constant high-speed flush mode whenever not integrating or reading out; a complete frame is erased in 87 ms.

The camera contains a programmable on-chip summing mode of N×M pixels that can be used to increase the cadence, improve signal to noise, and/or cope with telemetry limitations, sacrificing spatial resolution.

3.5. On-board Control and Processing Computer System

MDI's on-board computer system consists of two coupled but essentially independently operating units: the Dedicated Experiment Processor (DEP) and the Image Processor (IP). The DEP runs the science observing sequences that in turn control the IP, controls the electromechanical systems, maintains the cadence of normal observing, and handles the majority of the spacecraft

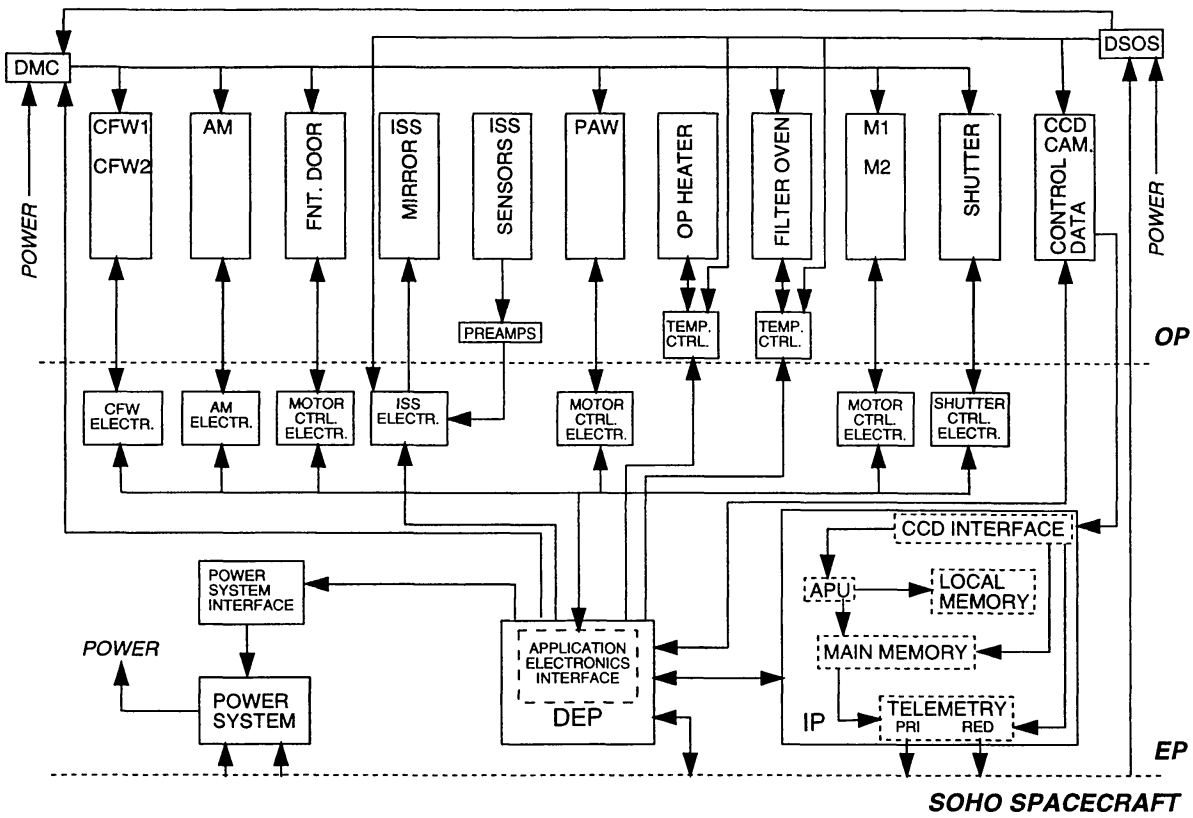

Fig. 11. Functional block diagram of the MDI electronic control system. Nearly all of the electronics are located in the EP, including the DEP, IP, mechanism controllers, and power system. The camera and some other noise-sensitive electronics are in the OP. The DMC (degraded motor controller) and DSOS (degraded science operations system) provide an independent means of controlling the instrument in case of catastrophic failure of the more complex systems.

interfaces, accepting spacecraft commands and sending back housekeeping and low-rate (5 kbps) science telemetry. The IP is essentially a high-speed, custom array processor. The DEP is based on 80C86 technology while the IP is based on 2900 series bitslice technology incorporated into application specific integrated circuits (ASICs) developed specifically for MDI. Figure 11 gives an overview of MDI's electronic systems.

The DEP contains 6 boards of electronics: (1) the CPU board, including opto-coupled interfaces to the thermal controllers, to the ISS, and to ground test equipment; (2) the memory board with 64 KB of EEPROM, 128 KB of RAM, and 4 KB of PROM; (3) the parallel interface board, which controls all the motors, the A/D interface, and the interface to the IP; (4) the CCD camera interface with shutter synchronization of integrate and readout commands; and (5,6) two spacecraft interface boards that handle spacecraft commands, the housekeeping and low-rate science telemetry. Its Intel 80C86 processor allows efficient development of the flight software on common PC's with a Borland C++ compiler.

The Image Processor (IP) is MDI's on-board data processing and reduction computer. It processes data from the camera to create observables, bins these observables (in time and space) into data products, and transfers these data products either to the spacecraft via its high rate telemetry interface or to the DEP for placement into the low rate science data channel. It consists of four subsystems for data processing, a DEP interface for system control, and 20 memory pages, each with 2.125 MB of RAM.

The IP's four processing subsystems are (1) a parallel arithmetic processor unit (APU) that contains a complex ASIC; (2) the main memory including a second ASIC that implements direct memory access (DMA) control for APU-independent data transfers, performing addition/subtraction, error detection and correction, as well sub-area extraction directly in the memory pages; (3) the CCD camera interface that directs the data flow, with a direct interface path between the CCD camera interface and the APU to provide additional redundancy; and (4) the telemetry interfaces (two redundant units) that pack the data and perform the first differencing and Rice encoding portion of lossless high-rate data compression.

The on-board software system for MDI involves the two coupled computers described above. The most challenging aspect of the MDI software is managing activities in several different time domains. Observations taken for each of the SOI observing programs, Structure, Dynamics, Campaigns, and Near Real Time Magnetic, must be woven together in a seamless fashion that maintains the temporal continuity of the helioseismology data. During normal operations, the DEP configures the optics and operates the camera in "real-time." Simultaneously the IP receives the previous camera frame, while also operating on data taken in the previous observing interval (minute). Furthermore, the DEP is acquiring data products from the IP that were created in the minute before that and transferring them to the spacecraft interface. In addition to this three-minute processing domain, the software is producing 24-minute time averages of various observables, taking regularly-spaced magnetograms that are stored for several hours before transfer to the ground, and managing a 24 hour circular buffer of low-ℓ velocity and intensity images.

In order to realize the temporal accuracy required for helioseismology, the DEP executes science observations in a highly synchronous fashion. Observations are defined by various lists. The most primitive list is the frame list. Other lists group these together to construct observations and campaigns. Each element in a frame list defines the time at which an image is to be taken and the associated instrument configuration. MDI Structure and Dynamics program observations are synchronized with international atomic time (TAI) and are centered on TAI minutes. Note that GONG observations are centered 5 seconds later, to account for SOHO's location at L_1.

The DEP commands the camera to take each filtergram image at the time indicated in the frame list. The time resolution in the DEP is 1/16 second with an accuracy of 1/2048 second. The DEP configures the instrument for the next frame upon completion of the camera readout. Prior to commanding the shutter and camera readout, the DEP places an IP command into a camera register. This command, actually a vector into the IP instruction queue, is sent to the IP along with the camera data.

Since the IP is operating in a different (i.e., more or less delayed) time domain, its operations are essentially independent of the DEP. The IP functions are controlled by programs in a hardware buffer named the instruction queue. The DEP also has access to the queue and loads its programs via telecommand. When the data transfer from the camera to IP memory is complete, the IP begins executing the program referenced by the vector. When the IP has completed a set of low rate data products, it issues an interrupt to the DEP. The DEP extracts data from a buffer in the IP and transfers it to the spacecraft telemetry system as packets become available.

3.6. Mechanisms

MDI has eight mechanisms and employs externally commutated brushless DC motors with rare-earth magnets operating in stepper-motor fashion (Akin *et al.*, 1993). The rotor/stator configuration is conventional. The rotors of the focus, polarization, and waveplate wheels contain optical elements.

The front door mechanism has two identical motors for redundancy. Either motor can open the door, but both must operate to close it.

The alignment mechanism consists of two motors. Each drives a spindle that moves a lever attached to one of the rear mounting legs. Driving the levers in unison raises and lowers the OP's rear, while driving the levers in opposite directions results in a side-to-side movement. The total range is approximately 800″ with 2″ steps. MDI will always point at Sun center.

The two calibration/focus wheels and the polarization analyzer wheel have 144 steps/revolution. Each has four positions for optical elements of 25.4 mm clear aperture.

The Michelson tuning motors rotate in 2 degree steps and have a repeatability of better than a few arcseconds; a systematic error of 1″ would produce a 5 cm velocity offset. Their design resembles the filter wheels, but each contains only a single optical element, a half-wave plate with a clear aperture of 50.8 mm, at the center of the rotor. Rotating the waveplate in conjunction with a fixed polarizer tunes the Michelson's passband.

The shutter motor spins a black anodized blade with a sector opening of 80 degrees, providing an unvignetted aperture. Exposures are taken by rotating the opening into the selected FD or HR path. Possible exposure times range from 40 ms to 16.4 s with 250 μs resolution. The absolute exposure

accuracy is 250 μs, but most importantly, exposure repeatability is better than 80 μs p-p, while the non-uniformity across the field of view is 50 μs p-p. Timing of the shutter exposure and the CCD integration are synchronized. Before each exposure the shutter blade moves to a fixed starting position. In doing so, the complementary light path falls on the CCD for 18 ms, so the camera flushes the resulting charge before the actual integration.

The MDI power system consists of two custom-designed 60 W switching power converters, each with a redundant backup. Either the prime or the redundant unit of each converter can be operated from either spacecraft power bus. The converters operate at 200 kHz and have post regulators for the critical voltages. The average load on each unit is approximately 15 W. Converter 1 powers the CCD Camera and the IP, while Converter 2 powers all of the other MDI subsystems. Each MDI subsystem can be turned on and off independently through actuated switches.

4. Observables and Performance

4.1. Observables and Measurement Techniques

To accomplish the SOI science objectives, MDI must produce measurements of line-of-sight velocity, line and continuum intensity, and magnetic fields. MDI records filtergrams, images of the solar photosphere in selectable, well-defined wavelength bands and polarization states. Because there is insufficient telemetry to transmit the number of filtergrams required to compute these observables at the cadence and resolution required, the observables must be computed by the instrument. The optical and processing systems described above provide the required images and processing. This section describes the algorithms used to compute the observable quantities.

Although the filter system does not perfectly isolate a single compact band of the spectrum, filtergrams have the characteristics of truly monochromatic images tuned through a solar line. Therefore, they can be treated like intensities at single wavelengths, rather than Fourier components of the entire spectrum (as is done for a Fourier tachometer such as the GONG instrument). The filtergrams are used to derive the six key observables listed in Table III. Estimates of the single measurement noise level are also given.

The standard observables are computed from sets of five filtergrams equally spaced by 75mÅ. They are labeled F_0 through F_4, with F_0 being nearly continuum, F_1 and F_4 centered on the wings and F_2 and F_3 centered about the core of the center-of-disk Ni line. The primary observable is the Doppler velocity. MDI derives an estimate of this from a ratio of differences of filtergrams F_1 through F_4:

$$\begin{aligned} \alpha &= (F_1 + F_2 - F_3 - F_4)/(F_1 - F_3), \text{ if numerator } > 0 \\ &= (F_1 + F_2 - F_3 - F_4)/(F_4 - F_2), \text{ if numerator } \leq 0 \end{aligned}$$

TABLE III
Observables, with noise levels for a one-minute measurement

OBSERVABLE	NOISE (1-σ)	FULL DISK	HI RES.
Doppler Velocity	20 m/s	Yes	Yes
Continuum Intensity	0.3%	Yes	Yes
Line Depth	0.7%	Yes	Yes
Longitudinal Magnetogram	20 Gauss	Yes	Yes
Horizontal Velocity	30 m/s (8 hours)	No	Yes
Limb Position	0.02″ (5 minutes)	Yes	No

The IP calculates the Doppler velocity from α using a lookup table constructed from simulations using parameterized solar line profiles and the measured filter transmission profiles. The lookup table and examples of systematic errors caused by various effects are plotted in Figure 12.

This velocity measurement has several noteworthy properties:

1. It is essentially blue wing minus red wing intensity divided by continuum minus line center intensity, so it is quite insensitive to variations in the slopes of the wing intensities.
2. It is independent of linear gain and offset variations in the intensity measurements, so raw CCD images can be used without penalty.
3. It is very insensitive to line depth but has modest systematic errors when the line width differs from the value assumed in constructing the table.
4. Additional errors are caused by Michelson mistuning and by miscentering of the Lyot filter with respect to the solar line. Since these effects are known and fixed within the instrument, they will be reduced considerably by the calibration procedures described in Section 4.3.
5. Systematic errors are generally less than ± 150 m/s over a range of ± 3000 m/s for the known variability of the solar line. However, the width-dependent errors rise steeply for velocities as large as ± 4000 m/s, which is approximately the velocity range encountered in MDI observations.

The line depth is the continuum minus line center intensity. It is estimated from the four filtergrams by:

$$I_{\text{depth}} = \sqrt{2\ ((F_1 - F_3)^2 + (F_2 - F_4)^2)}$$

This odd-looking formula is motivated by a discrete Fourier transform representation of the line profile as $I_{\text{cont}} - I_{\text{depth}}\ \cos(2\pi(\lambda - \lambda_0))$, assuming the four filtergrams are evenly spaced over one period. It reproduces the true

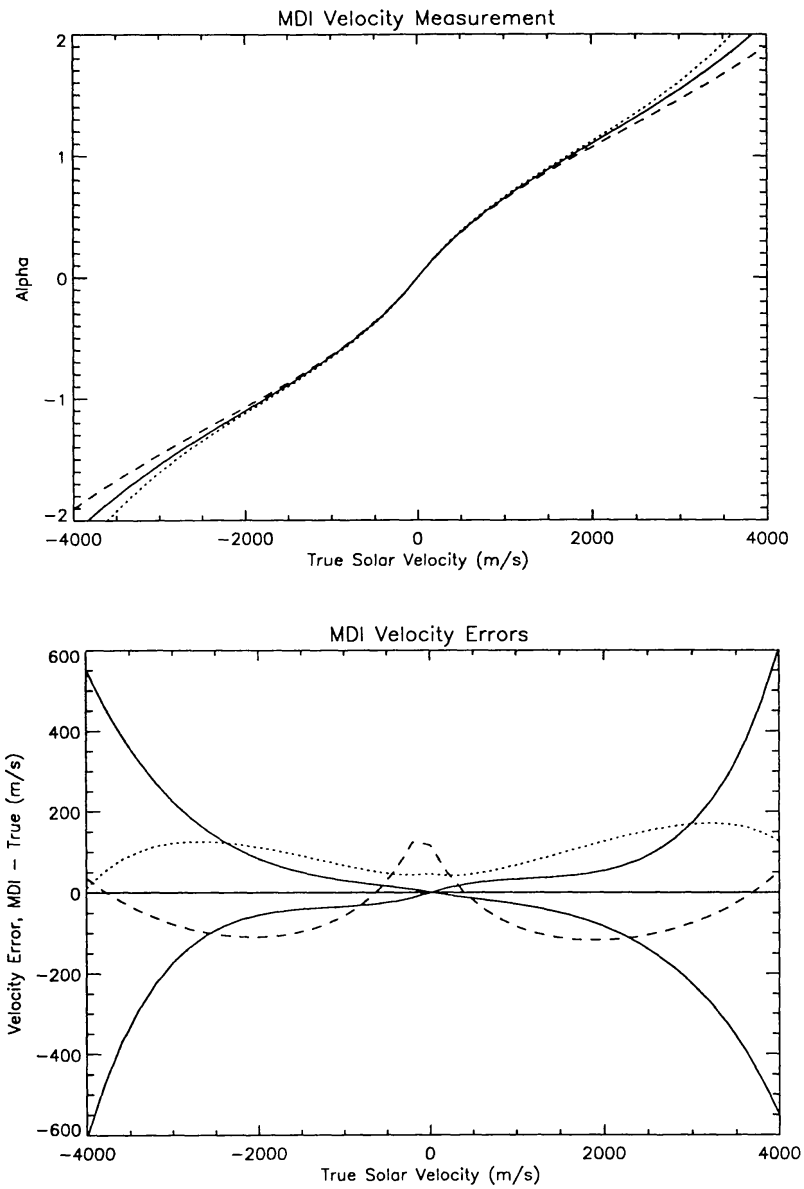

Fig. 12. The upper panel shows α versus velocity calculated for a nominal line profile (solid) and for lines 25% broader (dashed) and narrower (dotted). The lower panel shows velocity error versus velocity for a reasonable range of solar line profile and filter variations. The solid curves show the velocity error with perfect filters but line profiles that are 25% broader or narrower than the profile used to construct the velocity lookup table. The dashed line shows the effect of mistuning of the Michelsons, -10 mÅ for M1 and +30 mÅ for M2. The dotted curve shows the effect of a Lyot central wavelength shift of +75 mÅ relative to the nominal line center at zero velocity.

line depth to an accuracy of about 5% over the variation of line profiles and velocity considered above.

The continuum intensity is computed using all five filtergrams:

$$I_c = 2F_0 + I_{\text{depth}}/2 + I_{\text{ave}}$$

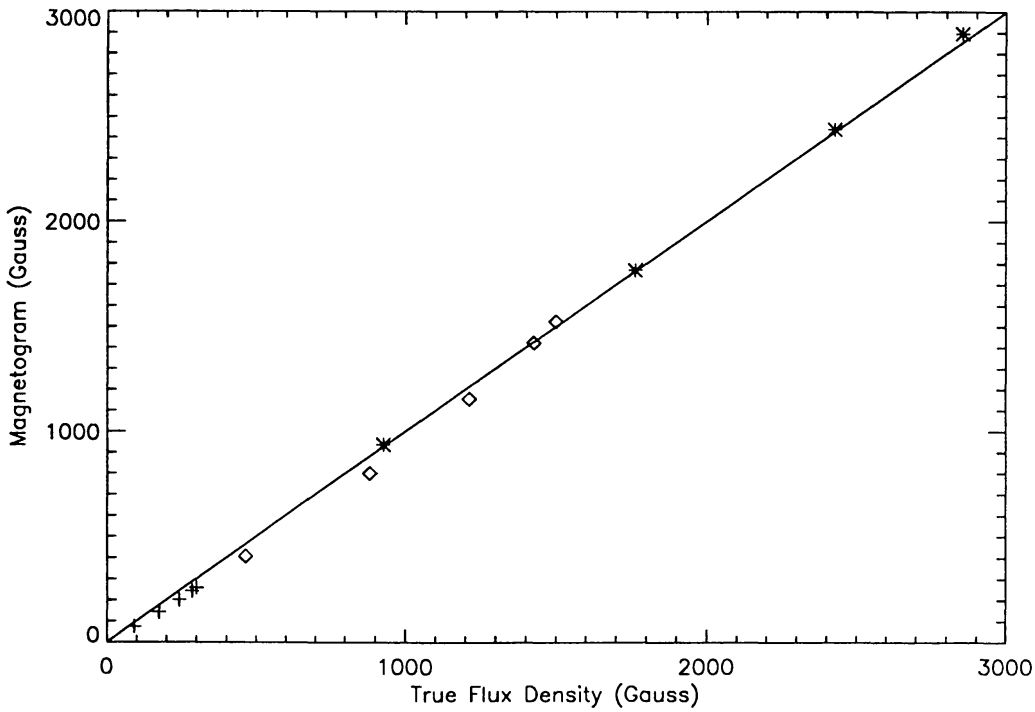

Fig. 13. Plot of modeled MDI magnetogram signal vs. true flux density, for umbral profiles (asterisks), penumbral profiles (diamonds), and plage profiles (plusses). The solid line is simply y=x.

where I_{ave} is the average of the other 4 filtergrams, F_{1-4}. The components of this sum have cancelling systematic errors as a function of solar velocity, so the result is a continuum image free from Doppler crosstalk at the 0.2% level.

A longitudinal magnetogram is constructed by measuring the Doppler shift separately in right and left circularly polarized light. The difference between these two is a measure of the Zeeman splitting and is roughly proportional to the magnetic flux density: the line-of-sight component of the magnetic field averaged over the resolution element. Figure 13 shows simulations of this magnetogram signal for sunspot and plage conditions, with various field strengths, inclination angles, and filling factors. These simulations use the same thermal line parameters in the magnetic and non-magnetic components. Differences cause an additional weighting factor of the unsplit equivalent width times continuum intensity (Rees and Semel, 1979).

The remaining observables are derived by ground processing of continuum images. Horizontal velocities are measured by local correlation tracking of granulation in high resolution images (November *et al.*, 1987; Title *et al.*, 1986; Bogart *et al.*, 1988). Feature tracking algorithms may also be used on continuum and line depth images (Strous, 1994). The limb figure (both limb position and slope of the limb darkening) as a function of azimuthal angle

is derived from fitting a profile to a 6-pixel wide annulus extracted from full disk continuum images (McWilliams & Kuhn, 1992).

4.2. On-Board Data Processing and Compression

MDI collects image data at a rate of 4.2 Mbit/s, but has telemetry allocations of only 160 kbps and 5 kbps. Each minute the image processor processes 20 raw filtergrams into two to four images of observables. Deletion of the off-limb pixels followed by compression permits transmission of complete full-disk velocity and continuum intensity images each minute when HRT is available. For high-resolution images, subimages of several observables may be sent, or one image at full resolution and a second at half resolution.

Velocity and magnetogram images are compressed in the IP using a lossless (i.e., reversible) algorithm. The first pixel in each telemetry frame is transmitted, followed by compressed first differences. The compression algorithm transmits k low-order bits unchanged, followed by n-k bits encoded using an efficient table; n and k are parameters chosen to optimize performance for each image type (Rice, 1979). Approximately 6-7 bits per pixel are needed for velocity and 5-6 for magnetic data. Additional compression is achieved on intensity images by taking a scaled square root before input to the n, k algorithm, resulting in 4-5 bits per pixel. Although this is not reversible, the difference between original and decompressed images is white noise whose variance is a fraction of the photon shot noise in the data.

The 5 kbps data channel, containing the Structure Program data, is always available and the IP uses data selection algorithms and weighted averaging in space and time to fill it to capacity. Gaussian smoothing functions are used to eliminate spatial aliasing in images and to filter p modes out of the time averages. Intensity images are corrected for offset and flat field and bad pixels are eliminated before binning. Table IV (Section 5.2) summarizes the Structure Program contents.

4.3. Calibration

A comprehensive series of performance and calibration measurements have been made by operating MDI in the laboratory for extended periods of time, recording thousands of CCD images in time series up to 11 hours long. The Sun, a continuum lamp, and a tunable laser have been used, along with various test patterns, jitter sources, etc., to calibrate the hardware elements. These measurements have included engineering characterizations of all subsystems described in Section 3. Even though subsystems were tested before installation, in most cases the definitive calibrations were completed during operation of the full flight instrument. The Sun was observed for many days, collecting filtergrams from which velocity, intensity, and magnetic fields were calculated. The quality suffers greatly from weather, seeing, pointing problems, software anomalies, interruptions, etc. Nevertheless, these data

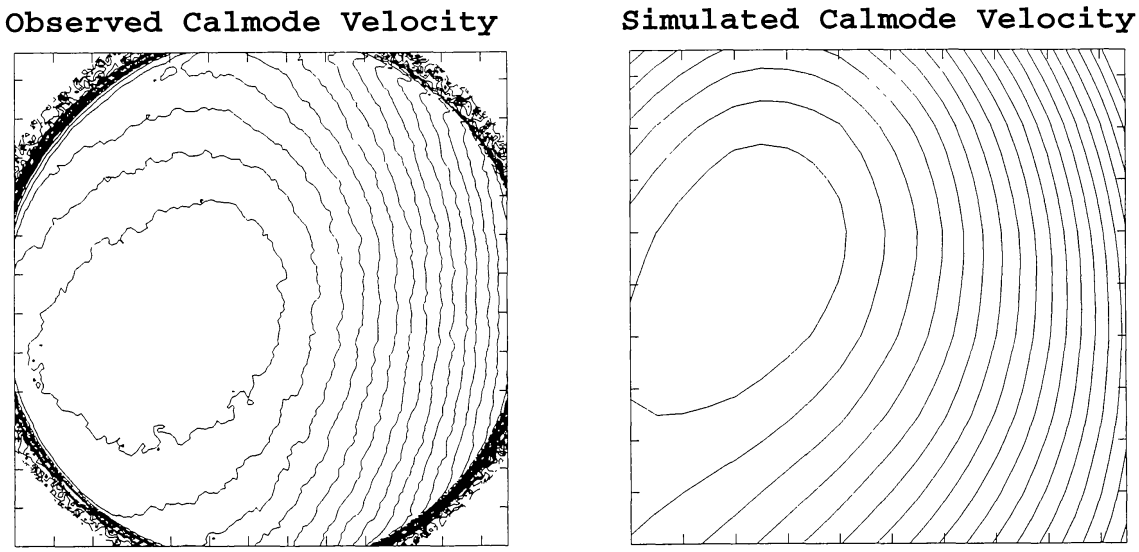

Fig. 14. Computed and measured CALMODE Doppler images. Contours are at 100 m/s intervals on the left and 70 m/s intervals on the right.

demonstrate the basic functionality of the instrument and emphasize how much better the SOHO environment will be for observing.

Stable imaging of the solar Doppler velocity was the prime design driver for MDI. The departures from near-perfect performance result mainly from wavelength gradients and angular dependence in the Michelsons and the summed transmission gradients of the optical elements. The primary calibration task is to produce the most accurate velocity measurements possible, correcting for instrumental imperfections and minimizing the effects of solar line profile variations. The four most critical instrument parameters are the central wavelengths of the Lyot filter and each Michelson and the final intensity at the CCD. Each ray of light traveling through the instrument encounters a different set of these parameters, and each pixel of the CCD integrates a different cone of rays during its exposure. Laboratory tests were performed to measure each of the four critical parameters in the four-dimensional space of rays (pixel location, x and y, and ray angle, θ_x and θ_y). We then incorporated these instrument properties into a mathematical model of the measurement process. This model predicts the measured velocity for known solar inputs and produces calibration curves and error estimates. In effect, the post-flight processing will use a unique velocity calibration curve for each pixel, derived using the instrument parameters and solar line profiles appropriate for its disk position. Figure 14 shows a CALMODE velocity image and the prediction from a preliminary version of the model. The model itself is calibrated by this comparison and

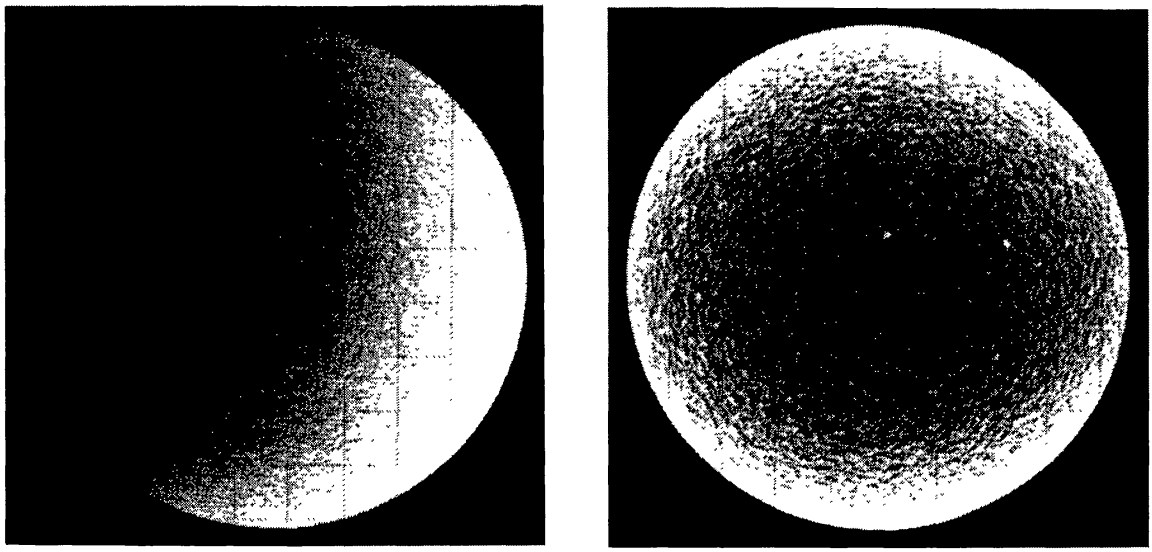

Fig. 15. Raw and corrected MDI Dopplergrams. Note the velocity features north of the equator, caused by active regions. The raw Dopplergram scale saturates at -800 and +2500 m/s; the corrected image scale saturates at -500 and +1000 m/s.

the model is then used to generate OBSMODE Doppler sensitivity and zero-point corrections.

In-flight calibrations will be performed regularly to measure changes from the laboratory characterizations. In CALMODE, maps of the Michelson central wavelengths and the peak transmission can be derived from a set of filtergrams with properly chosen tunings. These measurements are integrated over the cones of rays and so are not as complete as the laboratory versions obtained using a stabilized laser. Furthermore, they are affected by solar rotation, which causes a systematic Doppler shift across the ray cone for each pixel. This does not occur in OBSMODE. Additional information on this "colored cone" effect will come from data taken with the spacecraft rolled from the nominal position. Changes in the Michelson maps will be treated as perturbations to the preflight model when deriving the calibration curve for each pixel. A powerful check on calibration accuracy can be obtained by measuring velocities twice, first with the normal wavelength settings and then with a fixed, known wavelength offset; the velocities should always differ by the equivalent of the wavelength offset.

The imaging performance of MDI can be measured in flight using solar granulation as a test pattern for focus and image quality measurements. We will attempt to derive the optical transfer function of the instrument using the phase diversity technique of Carlson and Scharmer (1994). Intensity flat

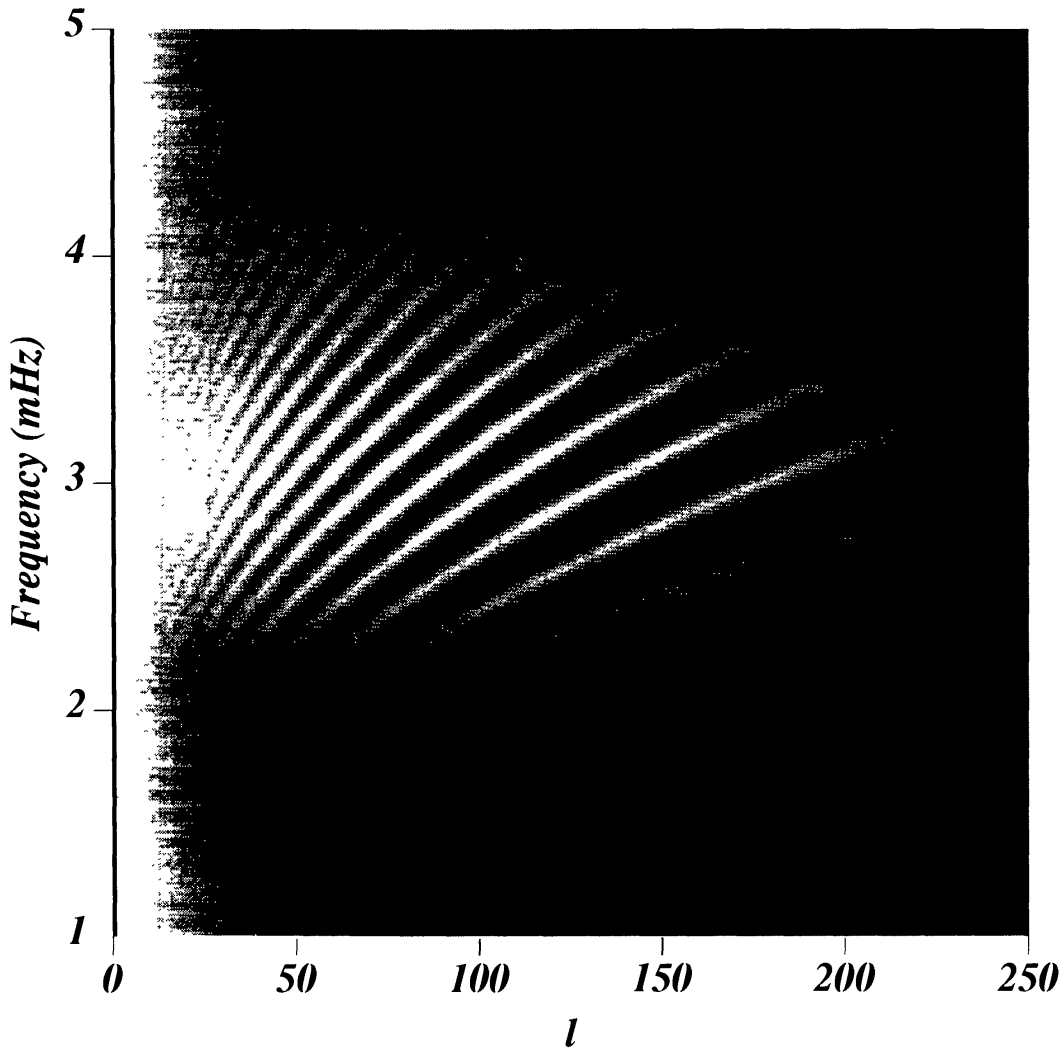

Fig. 16. $\ell - \nu$ diagram from 5 July 1993.

fields will be derived by the method of Kuhn *et al.* (1991) using sets of images offset spatially with the tilt mirror or alignment mechanism. The calibration mode image is a suitable target for CCD performance calibration.

4.4. Performance

Images of the MDI observables taken during testing show that the instrument performs as expected. The calibration mode velocity in Figure 14 has a gradient across it of about 1200 m/s, and the simulated image shows that this is expected from the filter performance. The raw solar velocity image (Figure 15) has a similar instrumental pattern, in addition to rotation and limb shift effects. The simplest possible correction, subtracting an average calibration mode velocity and a standard rotation profile, produces the image of Figure 15. This clearly shows supergranulation and oscillations, and an 11-hour time series of such images yields the quite acceptable power

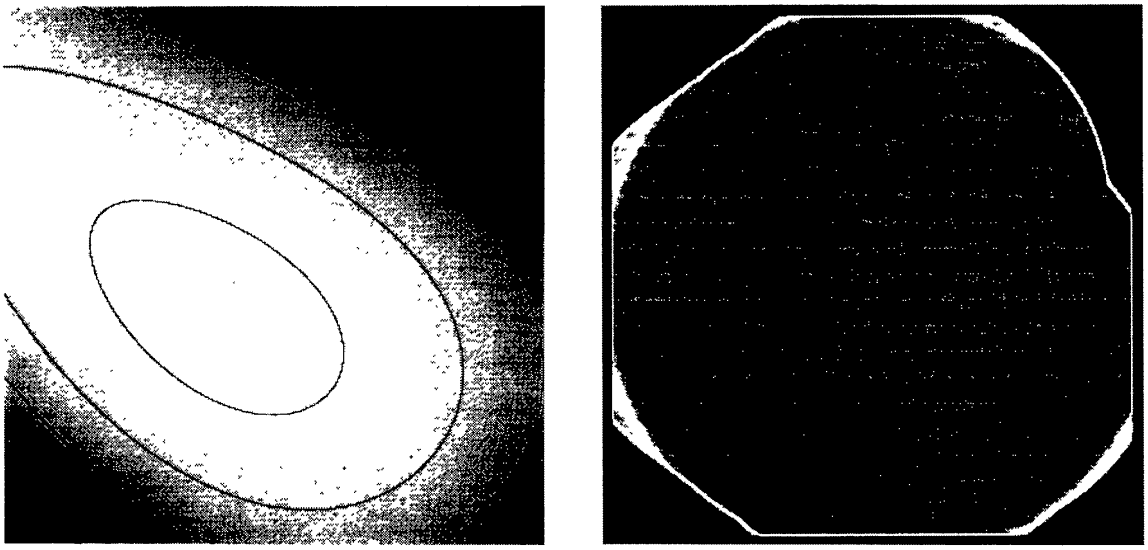

Fig. 17. The large-scale intensity gradient of the MDI optical path with 5% contours (left) and the detailed flat field correction image that saturates at ±2% (right).

spectrum ($\ell - \nu$ diagram) of Figure 16. The simulations show that such a zero-order correction removes 80 to 90 percent of the gradient, and the solar images are consistent with this. Corrected images still show some instrumental effects, especially near the limb, but the final calibration procedure should remove nearly all of this, and the residuals should be well- separated in frequency space from the p modes. The random noise level in a single velocity image is consistent with the 20 m/s rms level expected from photon shot noise plus 30 m/s from seeing and image motion; we expect flight data to be limited by photon noise.

Continuum intensity images and magnetograms were also made during testing. Figure 17 (left panel) shows the large-scale intensity gradient caused by nonuniform transmission in MDI's optical path, primarily due to the beam splitter cubes in the beam distribution box. This function plus the detailed flat field derived using the technique of Kuhn *et al.*(1991) (right panel) will be removed from the intensity images to correct for nonuniformities of the CCD chip. Flight data should have a shot noise of about 0.3% in a single measurement and residual flat fielding errors of a few tenths of a percent or less. Figure 18 shows an MDI magnetogram in high resolution mode and a Kitt Peak magnetogram of the same region taken the same day. Individual MDI flight magnetograms will have somewhat higher noise level (20 Gauss rms) than the KPNO data. The 2.3″ resolution of the KP data compares with the 4″ resolution of the MDI FD mode and the 1.3″ resolution of the HR mode.

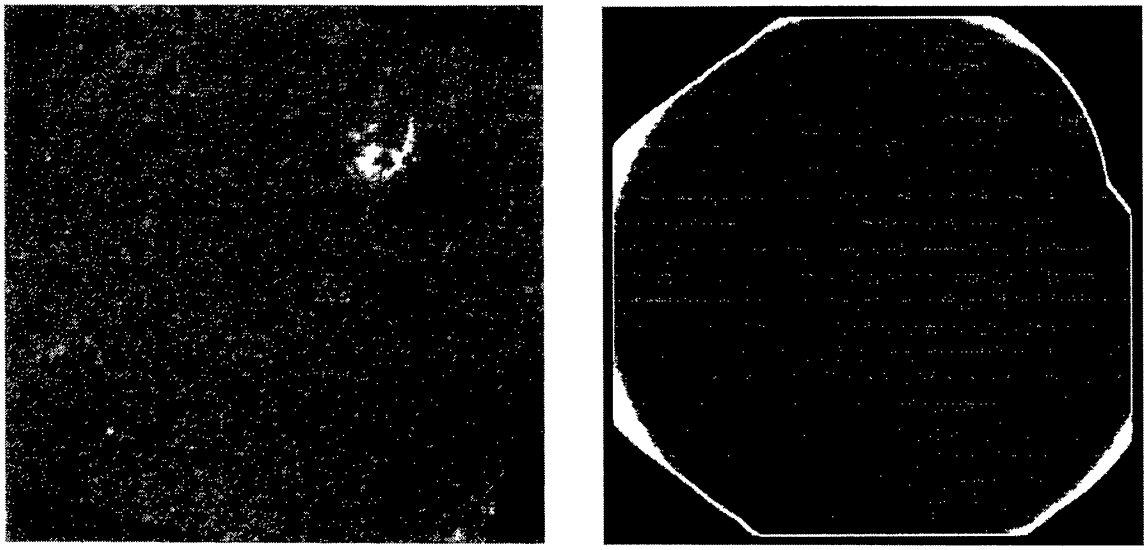

Fig. 18. High resolution magnetograms (MDI (left) & KPNO (right), taken several hours apart on 22 April 1994).

Ultimately, the scientific performance of MDI will be determined by the time dependence of the residual errors after calibration. Given the complexity of the calibration process and the analysis applied to helioseismology data, it is very hard to estimate the eventual levels of these errors in different parts of the spatial and temporal spectrum. MDI is made of high quality components, has been characterized in great detail, and will have a far more benign observing environment than other imaging helioseismology instruments. Unless the Sun is particularly malicious in its mix of solar oscillation signal and background noise, MDI should make very significant advances in all of its scientific objectives.

5. Scientific Observing Programs

The implementation of MDI science observing programs is fundamentally constrained by the amount of data that can be transmitted to the ground. The MDI observing programs are intimately tied to the different telemetry configurations available to the instrument. Two telemetry channels are available for MDI science data. The high-rate telemetry provides a 161840 bit per second channel which is referred to as the HRT or 160 kbps channel. The other, at 5022 bits per second, is the MDI share of the normal SOHO science data telemetry and is referred to as the LRT (low-rate telemetry) or 5-kbps channel. A third 300 bit per second channel contains the housekeeping data (HK) that indicate the status of the instrument. All SOHO data are captured by NASA Deep Space Network (DSN) telemetry ground

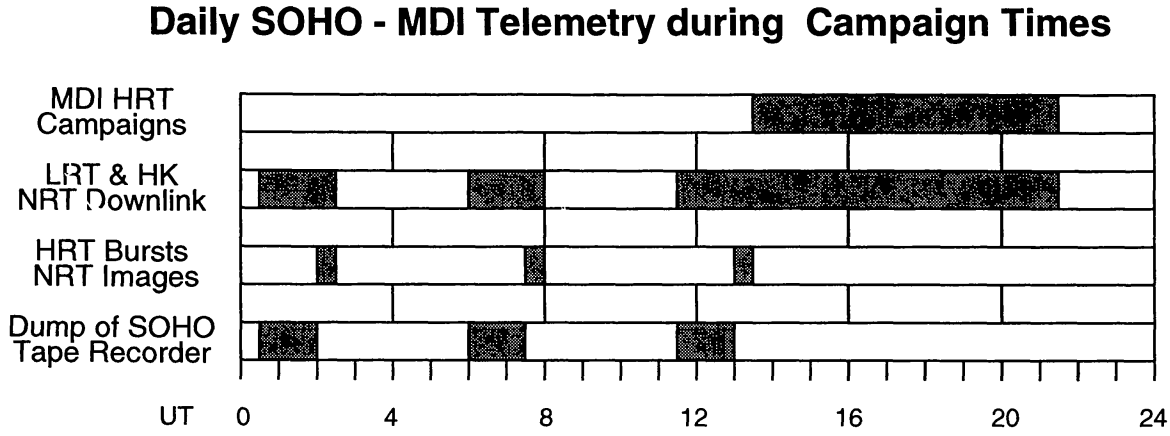

Fig. 19. Daily SOHO DSN coverage. SOHO provides for continuous coverage by recording the 5 kbps data on a tape recorder. MDI 160 kbps telemetry is available only during DSN passes after the tape recorder has been dumped. During the tape recorder playback and during MDI 160 kbps intervals, the 5 kbps data are transmitted directly to the EOF in near real time. A few minutes of MDI 160 kbps telemetry at the end of each of the three daily tape dumps is also forwarded to the EOF.

stations. Data received by the DSN are organized into virtual channels for different data handling and forwarding procedures. The MDI HRT data will be in one of two virtual channels, only one of which will be forwarded to the SOHO operations center in near real time. The other, containing nearly all of the MDI HRT data, will be mailed directly to Stanford on tapes. Figure 19 shows the daily SOHO telemetry schedule during Campaign intervals.

Nearly continuous coverage is maintained for the HK and 5 kbps channels. These data are available at the SOHO Experiment Operations Facility (EOF) shortly after receipt by the DSN. Only about 0.1% of the MDI raw data can be captured in the LRT channel. SOI will have approximately 8 continuous hours of 160 kbps telemetry each day during nominal operations, and continuous HRT during a scheduled 2-month interval each year. Most HRT data will be available to the SOI Science Support Center only after several days. Five- to 10-minute bursts of MDI HRT will be transferred directly to the EOF, usually just after the tape recorder playback. These near real time images will provide magnetograms and other images for daily SOHO science planning and allow immediate verification of instrument calibration and performance.

SOI's science operations have been organized into four programs that correspond to the various telemetry configurations. The following sections describe (1) the Dynamics Program that functions during the 2-month intervals of continuous HRT coverage, (2) the Structure Program that operates at all times using the 5 kbps channel, (3) Campaigns that run during the

daily 8-hour HRT intervals, and (4) the Near Real Time/Magnetic Program that takes advantage of the HRT that flows immediately to the EOF after the 3 daily tape dumps.

5.1. The Dynamics Program - 2 Months of Uninterrupted Solar Observations

The Dynamics Program produces the primary data set of the SOI program. The Dynamics Program is also the simplest because it requires the least on-board processing. During at least 60 consecutive days of continuous HRT, two complete images are transferred each minute. One of the images is the full-disk velocity data. The second image is either full-disk intensity or high-resolution velocity. To maximize the continuity of these data, the number of magnetograms taken each day will be limited to about three.

Analysis of 86,400 consecutive 1-minute cadence full-disk velocity images will enable us to determine the frequencies of the oscillations to better than 0.2 μhz. The Dynamics Program should provide our best data for characterizing the state of the convection zone because it provides complete coverage of all modes up to $\ell = 750$ and sensitivity to modes up to $\ell = 1500$ over a two rotation interval.

Full-disk continuum intensity data have a different resolution and signal-to-noise ratio for p modes than velocity observations, so the second image, during at least part of the 2-month intervals, will be FD I_c. Such images have increased sensitivity to mode properties near the limb; however, we may not allocate the entire 60-day interval to these observations. An alternate use for the second image in each minute is high-resolution velocity. High-resolution velocity images can provide unique data for understanding local convective phenomena. A likely scenario is that we will dedicate ten consecutive days at the beginning, middle, and end of the 60-day interval to full-disk intensity and the remaining two 15-day intervals to high-resolution velocity images. This would provide three time series of full disk intensity data sampling one range in longitude and two fifteen day datasets of high resolution velocity sampling another range in longitude.

Since the convective turnover time in the convection zone is comparable to the solar rotation period, we will have only a few samples of the largest-scale convective structures. It would be highly beneficial to extend this baseline. We have requested additional intervals of at least 80 hours of continuous HRT data spaced at 27-day centers before and after the 60-day intervals. One such 80-hour interval of Dynamics Program data will be available during the first 30 days of normal SOHO operations. We will use that data set to help demonstrate the usefulness of such intervals and to help select the mix of velocity and intensity images to use in the Dynamics Program.

The Dynamics Program will allow us to probe the zonally averaged structure of the full convection zone and to study local convective flows by mea-

suring the effect of waves propagating in an inhomogeneous medium. The Dynamics Program data will be one of the best data sets for understanding active regions, local convective motions, and large-scale flows. Comparison of data from one year to the next will show how the convection zone changes as the solar cycle progresses. These two months of continuous coverage will also serve to validate and refine the results of the Structure Program.

MDI full-disk observations will be sensitive to the solar oscillations of angular degree, ℓ, from 0 to approximately 1500. However, the modes of high degree cannot be resolved as individual peaks in oscillation power spectra because the frequency difference between the neighboring high-ℓ modes is smaller than their linewidths and also because of the inevitable leakage of the neighboring modes through the spatial spherical-harmonic filter due to our ability to observe only one hemisphere of the Sun. Since the high-degree modes are merged into ridges in the ℓ-ν diagram, their frequencies cannot be determined as accurately as the frequencies of modes of lower degree. In the best ground-based data the merging occurs at $\ell \simeq 180$. It is important to push this limit to $\ell \simeq 300$ to accomplish the scientific objectives formulated in Section 2, particularly for low-frequency modes which have relatively narrow line widths. This will require development of special analysis techniques in addition to the traditional ones described in Section 7.3.

5.2. The Structure Program - Continuous Coverage of Selected Spatial and Temporal Averages

The Structure Program runs at all times and fills the 5 kbps channel. It provides the only opportunity for long-duration continuous MDI observations. Priority for Structure Program telemetry goes to data contributing to science goals that require continuous coverage. Some of the telemetry will be reserved for oscillations with long lifetimes and low frequencies for which the longest possible observations are required. These data will provide the most accurate mode frequencies and probe the deepest into the Sun.

In order to meet the requirement of continuous Structure Program operation and still implement Campaigns, the observations must be interleaved in time. There are two Structure Program modes. Each produces the same data products from the computed velocity and flat-field corrected continuum intensity. One uses all 20 filtergrams collected during each whole minute and the other uses 10 filtergrams obtained in a 30-second interval. In both cases Structure Program observations are always centered on TAI minute marks. The 10-filtergram Structure Program runs when campaigns require a different set of filtergrams. The Structure Program presents the most difficult on-board programming challenge because of the number of data products and the level of processing required. Table IV lists the contents of the 5 kbps data stream.

TABLE IV
Structure Program Measurements in the 5 kbps Channel

Objective & Observable	Bins	Cadence (min)	% of telemetry
Medium-ℓ Velocity	18,600	1	86
Low-ℓ Velocity	64	1	<1
Low-ℓ Continuum Intensity	64	1	<1
Limb Figure Continuum Intensity	15,000	12	5
Flux Budget Continuum Intensity	128 x 128	12	4
Magnetic Proxy Line Depth	128 x 128	12	4

The largest component (86%) consists of about 20,000 weighted spatial averages of velocity. Specifying the spatial averaging determines the sensitivity to particular modes. Until several months after the first Dynamics Program run, the averaging bins are optimized to provide continuous coverage of modes up to ℓ of about 250. This is a simple rectangular sampling of the inner 90% of the disk with 12″ spacing and a 24″ FWHM Gaussian for anti-aliasing. This scheme has an effective resolution of 5×5 pixels, and will most clearly reveal the static long-term internal structure and dynamics of the Sun from the core out to 0.96 $R_\odot$. Slow changes in structure will also be visible. This binning is comparable to that of the GONG instrument and therefore is important for cross-calibrating GONG and MDI.

However, since the prime goal of MDI is to provide high-resolution data, we plan to switch to a nonuniform binning scheme that provides higher spatial resolution near the equator after several months. This second scheme, shown in Figure 20, will be sensitive to all zonal ($m = 0$) and sectoral ($m = \ell$) modes up to $\ell_{\max} \simeq 350$, but to only some modes of intermediate azimuthal orders m at the higher degrees. These higher-order modes do not penetrate deeply into the Sun, but are sensitive to structure in the He II ionization zone. The zonal and sectoral modes are of particular interest because the former provide information about the spherically symmetric structure of the Sun, and the latter continuously monitor the rotation and convection in the equatorial zone. It will be possible to apply other inhomogeneous binning schemes if higher resolution of a particular group of modes is required. Analysis of the first Dynamics Program data will aid in determining the particular averaging bins to use.

The continuum intensity in the pixels nearest the limb are ideally suited for detecting long-period low-ℓ modes and may provide SOI's best chance of detecting g modes. A 6-pixel annulus of limb pixels will be temporally averaged using a 24-minute Gaussian weighted window and sampled each

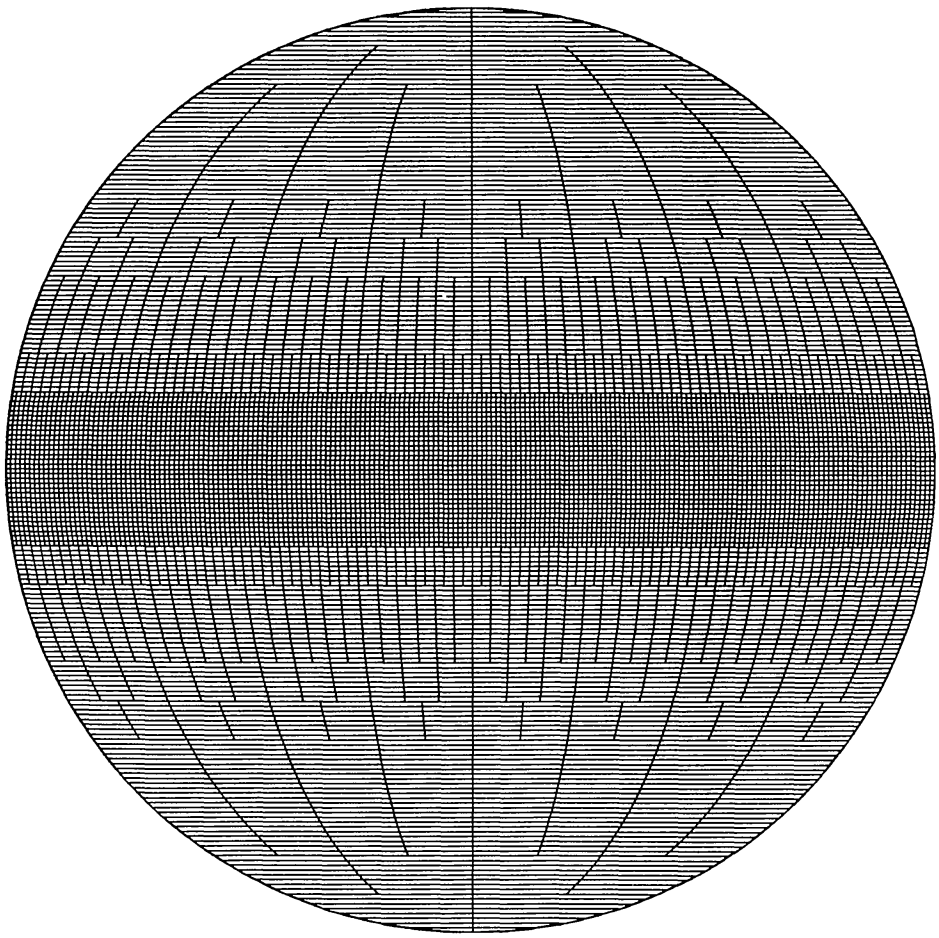

Fig. 20. A non-uniform binning scheme for the Structure Program designed to study subsets of high-degree modes whose spatial structures are close to zonal ($m = 0$) and sectorial ($m = \ell$). The modes of intermediate azimuthal degree will be observed with less resolution.

12 minutes. The limb data will also be used to provide the precise location of the CCD image for mapping to solar coordinates.

Data for several SOI science objectives will be supplied by series of two intensity-like images. To monitor the continuum flux budget 24-minute Gaussian weighted averages of continuum intensity will be computed on a binned 128^2 grid. A second similarly averaged magnetic field proxy will also be obtained. These lower-resolution images will be used for determining the variations in some systematic errors that are expected to contaminate the GOLF signal and to disentangle the contributions of sunspot and faculae to the total irradiance measurements made by VIRGO.

Finally, to measure low-ℓ modes, 64 super-pixels in velocity and continuum intensity are computed each minute. To best complement the VIRGO science analysis, the super-pixel averaging bins are exact quarters of the LOI science and guiding pixels. To maximize continuity, these low-ℓ data are also collected in a 24-hour ring buffer that is transmitted after each tape dump.

5.3. Campaigns - Daily 8-hour Observing Intervals

Observing sequences run during HRT intervals shorter than 80 hours are called Campaign Programs. MDI can be programmed to perform a variety of specific observations during campaigns. Sequences will be designed by investigators to meet scientific objectives that do not require long uninterrupted observing intervals. Campaigns run during the daily 8-hour HRT intervals and may specify up to 10 filtergrams per minute. Observations can be made in any of the polarizations, in full-disk or high-resolution mode, and in either OBSMODE or CALMODE. Nearly complete images of two quantities can be downlinked each minute or, alternatively, subarrays or spatial averages of a greater number of quantities can be computed and downlinked. Some limitations exist because of conflicting hardware requirements of the Structure Program.

Some examples of campaigns include continuous high-resolution magnetograms to examine emerging flux; simultaneous high-resolution observations of velocity and intensity to look for small-scale features and to compare results of correlation tracking and oscillation measurements; instrument diagnostics and calibrations, such as line scans or a CALMODE time series, to verify the performance and stability of the instrument; rapid series of filtergrams on a small region of the photosphere to look for rapid changes or variations with height in the atmosphere; repeated FD velocity maps to double the cadence of the structure program and look for higher frequency modes; and interspersed observations of the magnetic field and continuum intensity at both resolutions to look for associations with solar activity or coronal mass ejections.

On a few occasions early in the mission, before the Structure Program begins, it will be possible to use all 20 of the filtergrams and all of the computer resources for special campaigns. For example, we will explore the high frequency domain by making Dopplergrams every 20 seconds in high resolution mode for an extended interval; such higher-frequency oscillations are sensitive to conditions in the upper regions of the atmosphere.

5.4. Daily Real Time Images and the "Magnetic" Program

A limited number of images transmitted in the HRT channel are transferred immediately to the EOF. These data will come in a 5-minute HRT burst at the end of each of the three daily tape dumps and will include full-disk and high-resolution maps of velocity and continuum intensity in image mode and calibration mode, as well as stored magnetograms. The intensity and magnetic images obtained about 6 hours before the start of the daily long HRT interval will be SOI's main contribution to the SOHO summary data and will be used for daily SOHO operations planning. The velocity

TABLE V
SOI SCIENCE TEAMS

Internal Rotation (2-D inversions)
Structure Inversions
Ring Diagram Analysis for Convective Structures
Hilbert Transform Analysis for Convective Structures
Time-Distance Analysis for Convective Structures
Active Region Seismology
Low Frequency - GOLF Intercomparison
Low Frequency - VIRGO Intercomparison
Low Frequency - Limb Figure Analysis
Surface Flows & Structures (Correlation Tracking)
Surface Flows & Structures (Doppler)
Synoptic Magnetic Field
Coronal Magnetic Field
Summary Data (for SOHO Correlative Studies)

and intensity maps will be used for calibration and for monitoring MDI's performance.

Full-disk magnetograms will be recorded about every 90 minutes. When HRT is not available, they will be stored in MDI memory for downlink during the HRT bursts. Fewer magnetograms will be obtained during the Dynamics Program to minimize gaps in the helioseismology data. This complete homogeneous magnetic record will be an important resource for studying the magnetic flux budget, the evolution of magnetic field structures, large-scale photospheric flows, and solar rotation. It will also be useful for interpretation of MDI, GOLF and VIRGO velocity observations and for correlative studies with other SOHO and ground-based instruments.

6. Scientific Investigations, Data Policy and Mission Operations

MDI mission operations are planned to accomplish specific investigations related to SOI's scientific goals. All investigations will be performed either as part of a Team Science Working Group or as an Individual Investigation.

Some of the SOI science objectives will be addressed by concerted team efforts. In order to encourage such early efforts, Team Science Working Groups have been formed to develop observation specifications and analysis procedures and later to carry out the research and complete the initial publications (see table V). These teams focus on specific well-defined science objectives and analysis techniques.

All other SOI scientific research will be pursued as Individual Investigations; these include individual CoI studies, collaborations of CoIs with non-team Members, and approved independent studies by Associate Investigators (AIs). AIs are members of CoI groups and others who have a demonstrated interest in the SOI program. The selection of Individual Investigations will continue throughout the SOHO mission. Others may seek early access to the SOI data for educational or research purposes by submitting proposals and being selected for Individual Investigations. The procedure for developing investigations is described below.

With the exception of some overview papers, the results of research undertaken as part of the SOI program will be published by the investigator teams that do the research in a manner and time deemed appropriate by those teams. Thus the Team Science groups and Individual Investigation teams will write the papers resulting from their respective efforts.

SOI intends to provide the widest accessibility of the data at the earliest reasonable date. SOI CoIs will have immediate access to all MDI data for purposes of planning future observations and investigations. AIs will have similar access through collaborations with CoIs. In order to maximize the gain from limited resources, to allow orderly development of investigations, and to reduce redundancy of efforts, everyone receiving SOI data must agree to limit use of the data for research leading to publications to those efforts described in the approved, publicly available Team Science and Individual Investigation plans. This restriction on use for research leading to publication will apply for a limited time, usually less than one year from the initial availability of the data. SOI will make all calibrated Level-1 MDI data generally available within a year of its availability to the SOI project. The costs for such general distribution may need to be borne by the requester, depending on the availability of funds. SOI's data policy is consistent with the overall SOHO data policy and with NASA and ESA policies.

6.1. Development of SOI Investigations

To make best use of the observing capabilities of the MDI instrument and the resources of the SOI Science Support Center (SSSC), all SOI science investigations will proceed through a series of steps, from the initial concept through to analysis of data and publication of results.

Proposals submitted for an investigation will detail the science goals, required observations, data processing, and estimate the required analysis resources. Proposals will be evaluated for compatibility with SOI science goals, overlap with mission objectives and existing investigations, and resource requirements. Approved SOI investigations will be assigned a Local Coordinator to facilitate the development of a detailed Investigation Plan. A page linked to the SOI home page, http://soi.stanford.edu/, will be gener-

ated for each investigation to track its progress. The history will be updated as each step is completed.

Two key parts of the Investigation Plan are the descriptions of observations to be made by the MDI instrument and the processing to be performed by the SSSC. Required observation sequences will be developed and verified on the MDI Simulation System, a laboratory version of MDI. The analysis pipelines required for calibration and processing will be developed by the investigation team. Collaborative observations will be coordinated with other SOHO instrument teams, other spacecraft, or ground observatories. The completed Investigation Plan will be presented at an SOI Team Meeting where its priority will be assigned. The required observations will then be incorporated into the observing plan at a monthly SOI science planning meeting and times for the observations assigned.

Observation sequences will be converted to command uploads and sent to the MDI instrument. A test run of new observation sequences will be executed well before the real observation. Observations will typically be initiated by command files generated one to three days prior to the scheduled starting time, but adjustments in the observation schedule can be made based on solar conditions. The spacecraft commanding and MDI status will be monitored to verify that the observation functions correctly.

After receiving telemetry files, the SSSC will ingest the data, archive the datasets, and schedule the proper processing pipelines. The raw data will then be processed to obtain calibrated images and statistical descriptions of the data quality prepared.

The local coordinator and lead investigator will examine the data products and data quality summaries in order to certify the data for further analysis. When the final science data sets are made available to the lead investigator, a period for exclusive publication rights by the investigation team begins. The lead investigator must provide progress reports on the state of the investigation as well as scientific results at SOI team meetings.

6.2. Mission Planning

Various documents detail the mission planning and operations aspects of both the SOHO mission and the SOI-MDI project. The *SOHO Science Operations Plan* gives a top level description of the science activities associated with SOHO including operations planning, resource utilization, coordination of joint observing, and data exchange. The *SOI-MDI Mission Operations Plan* details the responsibilities of SOI personnel at the EOF and the SSSC and describes how planning and operations are coordinated. The *SOI-MDI Experiment Operations Plan* describes how the MDI instrument is operated and includes detailed descriptions of instrument commands and telemetry.

The overall SOI-MDI science and operations planning will be coordinated at Stanford University. Participants attending quarterly team meetings will

assess performance and scientific progress, allocate resources, and develop long-term observing priorities. SOI team members will also participate in monthly SOHO science planning meetings. Short-term observing priorities will be established weekly by staff at the SSSC. The MDI Observer, resident at the EOF at Goddard, will generate the weekly observing plan from the prioritized list, in coordination with the overall SOHO Activities Plan, and develop an instrument commanding schedule. The SSSC and the MDI Observer will communicate closely as daily adjustments are made to the SOHO observing plan and assessments are made of opportunities for collaborative studies based on solar conditions.

6.3. Observation Development

MDI observation sequences will be developed to carry out the specified observations. Most sequence development will be performed at the SSSC and verified using the MDI Simulation System. The Simulation System is a working version of MDI constructed of flight spares and engineering hardware that operates in a laboratory at LPARL. It provides the ideal testing platform for developing sequences and will be valuable for diagnosing problems in the flight model.

New or modified sequences must be converted to MDI memory loads and then to files compatible with the SOHO commanding system. Sequence builders will coordinate and compile sequence definition requirements, build sequences with the sequence construction tools, develop supporting on-board data tables, and communicate new and modified sequences to the MDI Observer. The SOI-MDI staff at the EOF will coordinate the execution of sequences on the flight instrument.

Analysis programs will be developed to process the data for each observing sequence. Most sequences will generate standard observables, but some may require special calibration procedures. Test data generated on the MDI Simulation System will be available for development of analysis programs.

6.4. Nominal Operations

Activation and checkout of the MDI instrument will be performed during the first month after launch. Several large data tables required for on-board calculations will be uplinked at the start of the mission. The tables will occasionally be updated as required by changes in objectives or instrument characteristics. MDI will use about 2 MB to store an intensity flat-field, which will take several days to uplink. The tables are stored in error-corrected memory that corrects single bit errors and detects double bit errors. Critical data will be stored in memories with keep-alive power to reduce the telemetry requirements and improve the instrument operation after a power failure.

About a month after launch the instrument will be operated in a calibration and sequence verification mode. After the initial verification is completed, MDI will begin science operations. We will first perform campaigns that would conflict with the Structure Program, before the halo orbit injection. Tests of spacecraft jitter, spacecraft roll, and spacecraft pointing stability will also be performed during the transfer trajectory. Final verification of the prime dynamics sequence will require an 80-hour interval of continuous MDI high rate telemetry.

Two SOI-MDI staff members at the EOF will support nominal day-to-day operations. Their tasks will include coordinating mission planning with the SSSC and representing the SOI-MDI team at EOF planning meetings. The SOI-MDI workstations in the EOF will be used to support instrument commanding, verify instrument health and safety, and make MDI data available to other instrument teams. Summary data will be extracted at the EOF and processed to produce magnetograms and continuum images for collaborative planning purposes. Data will be subjected to quick-look analysis at the EOF and transferred to the SSSC to monitor the science performance of the instrument. The EOF will normally be staffed only during normal working hours.

The principal mode of MDI operations will be to use delayed commands from an established command plan; thus real time commanding during normal operations will be minimal. The command plan will consist of a set of files containing a combination of direct instrument commands, MDI sequence initiation commands, and sequence loads. The files will contain headers with the targeted uplink time and will be submitted the day before the operations take place. Most SOI Campaigns will use existing DEP sequences already in MDI memory. Campaigns will change frequently.

Near-real-time commanding will occasionally be used to support checkout of new or modified sequences and image processor tables and for recovery and resolution of anomalies. For near-real-time commanding, the MDI Command Workstation will be enabled to allow direct submission of commands for uplink with a latency of less than 60 seconds.

7. Data Reduction and Analysis

MDI will generate slightly more than two-thirds of the scientific data bits from SOHO, amounting to nearly 300 Gigabytes per year of compressed raw telemetry. Furthermore, the nature of helioseismic data imposes special requirements for data analysis in that the raw data consist of long time series of high-resolution imagery; indeed, a set of 10^5 megapixel Dopplergrams occupying nearly 200 Gigabytes is in a very real sense a single datum for helioseismic inversion. The operation of the SOI Science Support Center (SSSC) for the processing, management, and distribution of this very

substantial quantity of data is thus a central and essential feature of the SOI project. Broadly speaking, the key tasks of the SSSC are the decoding of telemetry, the calibration of the data constituting the fundamental permanent science archive of the mission, the production of reorganized data sets for certain well-defined analysis suites, and performance of computations required for some analysis programs on behalf of the science teams. In addition, the Center will serve as the archive for all SOI data during the mission, since the bulk of the SOI data will not be archived at the SOHO Data Analysis Center. This means that the SSSC will have the additional responsibility of providing data to team members and guest investigators.

7.1. Description of SSSC Components

The computing facilities of the SSSC are divided into a production system, an analysis system, and several dedicated support systems. The production system, which runs in a special-purpose processing environment with full control of its own resources, is a Silicon Graphics Power Challenge configured with six R8000 300-MFLOPS processors, 2 GB of main memory, and about 400 GB of on-line striped disk storage. This system is reserved for the production of well-defined data sets, namely all of the Level 0 and Level 1 archival data products, Level 2 datasets required for team science analysis, such as spherical harmonic mode decompositions and flow fields from correlation-tracking, and specific Level 3 products resulting from (yet to be defined) analysis campaigns requiring powerful computing resources.

The analysis system is a second Silicon Graphics Challenge, with four R4400 75-MFLOPS processors, 768 MB of main memory, and about 100 GB of on-line disk storage. This system is available both for development and testing of the production pipelines and for general analysis in a normal login environment. As the data flow and processing requirements permit, it will be possible to reconfigure the analysis and production systems so that the analysis system has access to the faster processors and/or greater memory. There are also a number of smaller systems, mostly workstations, supporting interactive analysis and general work at the Center.

The production and analysis systems are served by an off-line data system under the control of the Data Storage and Distribution System (DSDS). The heart of this system is a pair of Ampex 410 DD-2 19-mm helical-scan tape systems, each consisting of a tape drive with a sustained transfer rate of 15 MB/s and a stacker holding seven 165-GB tapes. The system thus holds about 2 terabytes of data with random seek times of less than five minutes. There is also a Lago wheel with two Exabyte drives capable of holding 54 5-GB Exabyte tapes. This is predominantly for data import and export, since the 19-mm tape format is not in wide use in the scientific community. Information on the contents and location of the millions of images and ancillary data sets stored in the DSDS are maintained in an Oracle database.

The processing environment has four major components: the Pipeline Scheduler (PS) that determines the data processing requirements and configures and executes Pipeline Execution (PE) tasks; the Pipeline Execution process that performs the data processing as directed by the PS; the Data Storage and Distribution System (DSDS) that retrieves, stores, catalogs, and archives data products as requested by the PE; and a number of Analysis Modules, the processing modules run by the PE to create data products.

The Pipeline Scheduler is the top level operator interface for data processing. As various tapes and CD-ROMs of MDI telemetry data become available, the PS allocates and reserves the resources needed to process them. Processing occurs in various stages from the initial ingestion of the raw data through to the creation of high-level data products. The PS launches PE with various specification files that define the processing. The PS can be restarted after any major stage of the processing, in the event of failure.

The Pipeline Execution manages a group of analysis modules. The modules form a pipeline in that the output of one module is available as input to the next. PE sequences the data through the modules, providing input data locations, output data storage, and output data cataloging and archiving on behalf of the analysis modules through its interface with the DSDS.

All data produced by analysis modules run by PE are input and output in a disk farm managed by DSDS. Data migrate between disk and tape according to demand and age. Analysis modules request data from the database. Input data are staged to disk, and the module is informed of the location of the data by the DSDS.

The pipeline is built from Analysis Modules that implement independent processing algorithms An Analysis Module has a well-defined structure that encapsulates and standardizes system-dependent features such as I/O and communications between programs. Individual Analysis Modules can be executed in other environments than the PE. This not only aids in development, but permits the same programs run in the pipeline to be run in a test or exploratory analysis environment.

7.2. Data Processing Flow

The standard data reduction and analysis flow is organized into levels. Level 0 processing of raw data essentially consists of proper data sequencing, identification and rejection of duplicate or corrupted telemetry, decoding, and decompression.

Level 0 data are then calibrated into physical units; the calibration procedures constitute the Level 1 processing. The resulting Level 1 data products are typically the most basic scientifically useful data, i.e., those that can be analyzed without special knowledge of the instrument and operations. Nearly all Level 1 datasets produced by SOI will be Dopplergrams, magnetograms, and photograms.

Many scientific investigations can be conducted directly with Level 1 images. Many others require further Level 2 processing. In particular, classical helioseismic analysis requires the observables to be decomposed into frequencies of spherical harmonic mode amplitudes, while other inversions require comparable decomposition into different spatial basis functions. While Level 2 processing may often be conceptually straightforward and nearly independent of instrumental details, it does require specialized knowledge and experience in data quality assessment. Furthermore, the sheer quantity of data to be transformed render certain steps impracticable on all but specially designed systems. Performing the spherical-harmonic time-series analysis on continuous month-long datasets determines, to a great extent, the performance requirements of the SSSC computer system. We will be able to complete the initial processing of the more than 100 Gbytes of compressed telemetry from the 60-day Dynamics Program within 2 months of the end of the observations.

Further direct analyses, such as inversions and comparison with models, will require interactive work; we refer to this as Level 3 processing. This processing is not part of any pipeline, but once again the quantity of data to be analyzed and the accessibility of the data at the SSSC make the facility uniquely capable of supporting many such analysis programs. Thus the SSSC is designed to support major Level 3 processing as analysis campaigns: well-defined analyses leading directly to results publishable by either the whole team or specific sub-teams.

Data distribution and archiving during the mission are handled by the DSDS. Tools are provided to query the database and select data of interest. Requested datasets are exported either to local disk storage or written to 8mm tape. Some essential data products will be written on CD-ROMs, and duplicate archives of all pipeline data products will be maintained at Stanford University and at LPARL.

The precise volume of data products of each type and level of processing depends on the actual mission observing schedule and on the mix of observations completed. Each year MDI will generate about 274 Gb of raw data; 18 in the Structure Program. From this, about 540 Gb of Level 0 data will be derived, including about 196 Gb for the Dynamics Program and 326 for Campaigns. The calibrated Level 1 data will take up slightly more space, 620 Gb. We estimate about 1500 Gb for Level 2 data products, about 300 for spherical harmonic mode parameters and most of the rest for other transform methods. The total annual predicted data volume is 2.9 Tb. The estimates neglect possible savings afforded by compression, which could be on the order of 50%. The difference between estimated sizes at Level 0 and Level 1 comes from assuming higher precision of intensity measurements after flat-fielding. The estimates for Level 2 data products, in particular, are highly uncertain.

7.3. Analysis Suites

The Level 0 processing of raw telemetry into sorted data products relies primarily on information contained in MDI camera headers, that describe the states of the instrument, and onboard processor and telemetry packet headers and command histories. Separate algorithms are necessary for the high-rate and the low-rate telemetry because the packet structures and compression techniques are different.

Calibration (Level 1 processing) procedures are undergoing intensive development. The primary task is to develop a suitable technique for velocity calibration using CALMODE data, housekeeping data, and models of the optical characteristics of the filters. Calibration of magnetic measurements is not expected to involve any additional problems apart from those normally involved in the interpretation of Zeeman splitting observations. Flat-field corrections to intensity measurements are based on the procedure of Kuhn *et al.* (1991).

Quality assessment procedures associated with the various types of Level 1 processing, along with the description of ancillary data and keyword requirements, are determined by the requirements of individual Level 2 and Level 3 processes.

Significant Level 2 processing procedures currently identified include traditional helioseismic processing, ring-diagram analysis for convective structures, and correlation tracking for mapping of surface motions. These are described below. Additional development is proceeding on a number of experimental procedures such as Hilbert Transform analysis, Time-Distance analyses, tracking of features identified by pattern recognition techniques, and coronal field extrapolation. Some straightforward procedures, such as preparation of animation sequences and synoptic maps for visual and numeric analysis, will also be implemented.

For traditional helioseismic processing, the calibrated images are apodized, remapped and projected onto all spherical harmonics with degree below some maximum. Transposing this dataset yields a collection of time-series of spherical harmonic coefficients. The prime analysis of these time-series will use Schou's (1992) method that results in tables of mode parameters for each interval. The tables will include mode frequencies, amplitudes, linewidths, line asymmetry parameters, estimates of the background noise, and various quality parameters. The mode frequencies will either be in the form of individual mode frequencies or parameterized using a-coefficients (e.g., Schou *et al.*). When possible, estimates of the statistical errors of the estimated parameters will be provided, including covariance matrix estimates.

The mode frequencies can be used to infer the internal properties of the Sun using inverse methods. As part of the team science we will perform inversions for both the radially averaged structure and the internal rotation

as a function of radius and latitude. The inversions for the radial structure will be performed using a variety of methods including variants of the Optimally Localized Averages and Regularized Least Squares (RLS) methods. The inversion for the rotation rate will be done using both a 1.5-dimensional and a 2-dimensional RLS method, as described in Schou *et al.* (1994).

Another processing procedure is ring diagram analysis that uses observations of either the full Sun or a sufficiently large region of the high-resolution field (Hill 1988). This technique involves performing a three-dimensional spatial-temporal Fourier transform of a small co-moving area on the Sun for plane waves, measuring the displacement and distortion of the surfaces of maximum power in the transform (whose cross-sections at a given temporal frequency are very nearly a set of concentric rings), and inverting the displacement and distortion parameters to obtain information about the fluid flow through which the acoustic waves are being advected. The ring fitting procedure to be used is currently problematic because existing algorithms are too inefficient to keep pace with the data flow (Patron, 1994; but see Bogart *et al.*, 1995).

A third procedure for determining surface flow velocities is correlation tracking of solar granules. In its high-resolution mode, MDI has sufficient spatial resolution to be able to statistically track the motions of granulation features (Bogart *et al.*, 1988). Surface flows will be calculated for Campaign sequences of high-resolution filtergrams using the techniques described by Simon *et al.* (1988) and November *et al.* (1987).

8. Conclusion

The Solar Oscillations Investigation will probe regimes of the solar interior inaccessible to any other program, particularly in the upper convection zone that influences all helioseismic phenomena. MDI will provide the first space observations of intermediate- and high-degree solar oscillations and is the first spaceborne solar magnetograph. Complemented by VIRGO and GOLF on SOHO and by GONG and other groundbased observations, we will characterize the complete structure of our nearest star with high accuracy.

MDI makes uninterrupted measurements of Doppler velocity and the continuum intensity with $4''$ resolution over the full solar disk each minute. Continuous telemetry is provided for a subset of spatial averages, but extended intervals of continuous complete coverage are planned. Frequent magnetic field and intensity maps will characterize the disposition of photospheric magnetic fields, improve the interpretation of helioseismology data sets, and supply planning data for other investigations. Flexible observing programs run during daily 8-hour Campaign periods will provide other useful data sets at either $1.25''$ or full-disk resolution.

Design of the hardware and software needed to make these observations and fit them into the allocated telemetry stream was a challenge; the software development is continuing. Prelaunch calibration of the instrument has been completed and the noise levels are consistent with obtaining photon noise and solar noise limited observations of the Doppler velocity. The major sources of systematic error are due to fixed pattern nonuniformities in the spectral filters and large-scale spatial intensity gradients. The errors are well characterized and mostly removable; in any case they are temporally stable and should not affect the measurements of oscillations. Complications due to variations in the solar line profiles are more problematic, but we can make diagnostic measurements of the error sources.

The SOI Science Support Center will be able to keep pace with the data flow, producing calibrated observables and completing standard scientific processing of the data, such as identification of mode frequencies. An independent computer system and distributed resources will provide significant capabilities for exploratory scientific analysis. Management and archival of the more than 3 TB of data produced each year are important functions of the SSSC.

Observations will generally be planned well in advance and will emphasize continuity to provide the maximum mode frequency precision. However, significant flexibility is allowed in the daily Campaign Programs. Observing sequences will be designed to provide the standard observables in either resolution, subject only to the restrictions imposed by the concurrent operation of the Structure Program and telemetry limits. Proposals for Campaign Observations and for Analysis Campaigns using extant data are welcome.

General information on the SOI program is available on the World Wide Web at URL http://soi.stanford.edu/. Included will be information on the status of all observing and analysis campaigns, and forms for querying the Data Storage and Distribution System for the availability of data. Individual investigation proposals and data requests will also be handled through this mechanism. The Web pages also include listings of SOI Technical Notes and other related publications that provide detailed information on all aspects of the investigation.

9. Acknowledgments

Development of an instrument of this complexity and of the required data processing capabilities involves a major commitment by members of a substantial team over many years. The authors gratefully acknowledge the important contributions of their colleagues, subcontractors and suppliers, and of NASA and ESA. In particular, this program has been supported financially by NASA under contract NAS5-30386 and programmatically by the invaluable cooperation of J. Gervin, D. Galoppo, D. Machi, R. King, and K.

Sizemore from the GSFC ISTP Project Office, and M. Calabrese, W. Wagner, and J.D. Bohlin at NASA Headquarters. D. Bock, of ESA, has been a key partner in accomplishing the goals of SOI-MDI throughout the program.

The Lockheed team responsible for the mechanical, optical, and filter subsystems included C. Abato, R. Cardenas, T. Cruz, K. Gowen, L. Huff, B. Jurcevich, N. Katz, K. Mitchell, T. Pope, L. Tavarez, D. Torgerson, and J. Vieira. D. Akin was responsible for the mechanisms. B. Choudhury and S. Morrison were responsible for the thermal control subsystems. The flight and ground software were developed by R. Chevalier, K. Goddard, M. Levay, D. Mathur, M. Morrison, and R. Rehse. B. Caravalho, J. Dusenbury, C. Edwards, R. Lindgren, D. McClurg, J. Suty, E. Thomas, and K. Zickuhr designed and produced the electronics; including the IP firmware (Lindgren). The CCD camera was developed by D. Duncan, G. Kelly, and M. Morrill. Performance assurance activities were led by E. McFeaters and L. Reynolds; contamination control by T. Rigney and M. Yee; and programmatics by D. Cauffman, F. Friedlaender, G. Gradwohl, B. Jaynes, J. Johnsen, J. Stephenson, and S. Taylor. C. Feinstein was the lead test engineer.

The Stanford team responsible for development of the SSSC has included J. Aloise, L. Bacon, K. Leibrand, V. Johnson, L. Sá, K. Scott, and J. Suryanarayanan. S. Williams developed much of the mission operations concept. P. Milford coordinated the development of specifications for the on-board processing. We also thank J. Lepetich, G. Morales, and M. Stehle for their important contributions.

We wish to acknowledge the people working with the SOI Co-Investigators, and in particular the efforts of the GONG team.

We are thankful for the excellent teamwork and technical performance of several of our subcontractors, including: Michelson Interferometers by Interoptics (J. Wimperis), CCDs by Loral Aeroneutronic (D. Bredthower), ASICs by LSI Logic, filters by Andover Corp. (R. Bennett and J. Cotton), birefringent crystals by Inrad Corp. (W. Ruderman), waveplates by Kappler Crystal Optics (R. Kappler), and mechanisms by H. Magnetics (R. Horber).

References

Akin, D., Horber, R., and Wolfson, J.: 1993, *NASA Conference Publication* 3205, 219.

Appourchaux, T., and Andersen, B.N.: 1990, *Solar Phys.* **128**, 91.

Bogart, R.S., Ferguson, S.H., Scherrer, P.H., Tarbell, T.D., and Title, A.M.: 1988, *Solar Phys.* **116**, 205.

Bogart, R.S., Sá, L.A.D., Duvall, T.L. Jr., Haber, D.A., Toomre, J., and Hill, F.: 1995, in V. Domingo, A. Poland, and J.T. Hoeksema (eds.), *Proceedings of the 4th SOHO Workshop: Helioseismology*, ESA SP-376, in press.

Braun, D.C., Duvall, T.L. Jr., and LaBonte, B.J.: 1988, *Astrophys. J.* **335**, 1015.

Brown, T.M.: 1980, in R.B. Dunn (ed.), *Solar Instrumentation: What's Next?*, National Solar Observatory: Sunspot, NM, 150.

Claverie, A., Isaak, G.R., McLeod, C.P., van der Raay, H.B., and Roca Cortés, T.: 1979, *Mature* **282**, 591.

Deubner, F.L.: 1975, *Astron. Astrophys.* **44**, 371.
Domingo, V., *et al.*: 1995, *Solar Phys.* , this issue.
Duvall, T.L. Jr., Harvey, J.W., Jefferies, S.M., and Pomerantz, M.A.: 1991, *Astrophys. J.* **373**, 308.
Evans, J.W.: 1980, in R.B. Dunn (ed.), *Solar Instrumentation: What's Next?*, National Solar Observatory: Sunspot, NM, 155.
Field, G.B., and the Astronomy Survey Committee: 1982, *Astronomy and Astrophysics for the 1980's*, National Academy Press: Washington, D.C.
Fröhlich, C., and the VIRGO Team: 1995, *Solar Phys.* , this issue.
Gabriel, A., and the GOLF Team: 1995, *Solar Phys.* , this issue.
Gough, D.O. and Toomre, J.: 1991, *Ann. Rev. Astron. Astrophys.*, **29**, Annual Reviews, Inc.: Palo Alto, CA, 627.
Grec, G., Fossat, E., and Pomerantz, M.: 1980, *Nature* **288**, 541.
Harvey, J., and the GONG Instrument Development Team: 1988, in E.J. Rolfe (ed.), *Seismology of the Sun and Sun-Like Stars*, ESA: The Netherlands, 203.
Hill, F.: 1988, *Astrophys. J.* **333**, 996.
Krimigis, S.M., and the Space Science Board Committee on Solar and Space Physics: 1985, *An Implementation Plan for Priorities in Solar-System Space Physics*, National Academy Press: Washington, D.C.
Kuhn, J.R., Libbrecht, K.G., and Dicke, R.H.: 1987, *Nature* **328**, 326.
Kuhn, J.R., Lin, H., and Loranz, D.: 1991, *P.A.S.P.* **103**, 1097.
Kumar, P., Duvall, T.L. Jr., Harvey, J.W., Jefferies, S.J., Pomerantz, M.A., and Thompson, M.J.: 1990, in Y. Osaki and H. Shibahashi (eds.), *Progress of Seismology of the Sun & Stars*, Springer-Verlag: Berlin, 87.
Kumar, P., and Lu, E.: 1991, *Astrophys. J. Lett.* **375**, L35.
Leibacher, J.W. and Stein, R.F.: 1971, *Astrophys. J. Lett.* **7**, 191.
Leighton, R.B., Noyes, R.W., and Simon, G.W.: 1962, *Astrophys. J.* **135**, 474.
Loefdahl, G. and Scharmer, G.B.: 1994, *Astron. Astrophys. Suppl.* **107**, 243.
McWilliams, T. and Kuhn, J.R.: 1992, *SOI Technical Note 83*, Stanford, CA.
November , L.J., Simon, G.W., Tarbell, T.D., Title, A.M., and Fergusen, S.H.: 1987, in G. Athay & D.S. Spicer (eds.), *Theoretical Problems in High Resolution Solar Physics II*, NASA Conf. Publ. 2483: Washington, D.C., p. 121.
Noyes, R.W., and Rhodes, E.J. Jr., eds.: 1984, *Probing the Depths of a Star: The Study of Solar Oscillations from Space*, NASA JPL: Pasadena, CA.
Patrón Recio, D.J.: 1994, *Tridimensional Distribution of Horizontal Velocity Flows Under the Solar Surface*, Ph.D. Diss., Inst. de Astrofísica de Canarias: La Laguna, Spain.
Rees, D.E. and Semel, M.D.: 1979, *Astron. & Astrophys.* **74**, 1.
Rice, R.F.: 1979 in *SPIE Symp. Proc.*, **207**, San Diego, CA.
Schou, J.: 1992, *On the Analysis of Helioseismic Data*, Ph.D. Dissertation, Aarhus Universitet: Aarhus, Denmark.
Schou, J., Christensen-Dalsgaard, J. and Thompson, M.J.: 1994, *Astrophys. J.* **433**, 389.
Simon, G.W., Title, A.M., Topka, K.P., Tarbell, T.D., Shine, R.A., Ferguson, S.H., Zirin, H., and the SOUP Team: 1988, *Astrophys. J.* **327**, 367.
Spruit, H.C., Nordlund, A., and Title, A.M.: 1990, *Ann. Rev. Astron. Astrophys.* **28**, 263.
Strous, L.H.: 1994, *Dynamics in Solar Active Regions: Patterns in Magnetic-Flux Emergence*, Ph.D. Dissertation, Universiteit Utrecht: Utrecht, The Netherlands.
Title, A.M. and Ramsey, H.E.: 1980, *Applied Optics* **19**, 2046.
Title, A.M. and Rosenberg, W.J.: 1979, *Applied Optics* **18:20**, 3443.
Title, A.M. and Rosenberg, W.J.: 1981, *Opt. Eng.* **20:6**, 815.
Title, A.M., Tarbell, T.D., and Simon, G.W.: 1986, *Adv. Space Res.* **6**, 253.
Title, A.M., Tarbell, T.D., Topka, K.P., Ferguson, S.H., Shine, R.A., and the SOUP Team: 1989, *Astrophys. J.* **336**, 475.
Ulrich, R.K.: 1970, *Astrophys. J.* **162**, 933.
Zayer, I., Chapman, I., Duncan, D., Kelley, G., and Mitchell, K.: 1993, in *SPIE Symp. Proc.*, **1900**, 97.